Nonlinear Dyn (2025) 113:32979–33004
https://doi.org/10.1007/s11071-025-11781-1

RESEARCH

Hybrid GA-IPA and neural network-based solution for fractional-order nonlinear predator-prey dynamical systems

Nassira Madani · Zakia Hammouch · Necati Ozdemir

Received: 7 March 2025 / Revised: 21 August 2025 / Accepted: 2 September 2025 / Published online: 29 September 2025

Abstract This paper proposes a novel approach for solving fractional-order nonlinear predator–prey dynamical systems using artificial neural networks (ANNs), with the goal of improving accuracy and computational efficiency in modeling complex real-world ecological interactions. A hybrid computational intelligence framework is developed, integrating ANNs with a Genetic Algorithm–Interior Point Algorithm (GA–IPA) for parameter optimization. The ANN serves as the modeling core, while the GA–IPA optimization refines network parameters to achieve high precision and stability. Numerical simulations confirm that the proposed ANN–GA–IPA approach effectively captures the dynamics of the fractional-order nonlinear predator–prey system. The method demonstrates strong robustness and high accuracy, outperforming conventional techniques in representing dynamic ecological behaviors. This work introduces, for the first time, the application of a hybrid ANN–GA–IPA strategy to fractional-order dynamical systems, delivering improved computational performance and modeling accuracy, offering a powerful tool for analyzing complex biological interactions and presenting potential extensions to other classes of nonlinear systems.

Keywords Nonlinear predator-prey system · Fractional calculus · Artificial neural network · Genetic algorithm · Interior point algorithm

N. Madani
Faculty of Sciences Dhar El Mahraz, Sidi Mohamed Ben Abdellah University, LAMAA, Fez, Morocco

Z. Hammouch (✉)
Department of Mathematics, Saveetha School of Engineering, Saveetha Institute of Medical and Technical Sciences, Chennai, Tamilnadu 602105, India
e-mail: z.hammouch@umi.ac.ma

Z. Hammouch
Interdisciplinary Laboratory for Modeling Simulation and Scientific Innovation (LIMSIS), École Normale Supérieure, Moulay Ismail University of Meknès, Meknès 50000, Morocco

Z. Hammouch
Department of Medical Research, China Medical University Hospital, Taichung, Taiwan

Z. Hammouch
Department of Mathematics, Kyung Hee University, 26 Kyungheedae-Ro, Dongdaemun-Gu, Seoul 02447, South Korea

Z. Hammouch
Department of Mathematics and Applied Mathematics, School of Science and Technology, Sefako Makgatho Health Sciences University, Ga-Rankuwa, South Africa

Z. Hammouch
Jadara University Research Center, Jadara, Jordan

Z. Hammouch
Laboratory of Intelligent Systems Energy and Sustainable Development, Private University of Fez (UPF), Fez, Morocco

N. Ozdemir
Department of Mathematics, Faculty of Arts and Sciences, Balikesir University, Balikesir, Turkey
e-mail: nozdemir@balikesir.edu.tr

1 Introduction

Nonlinear systems, often referred to as complex systems, provide some of the most accurate representations of real-world phenomena due to their ability to capture intricate and dynamic interactions. Among these, the predator-prey model, originally introduced by Vito Volterra and Alfred Lotka in the early 20th century, stands as a fundamental example. Known as the Lotka-Volterra system, it describes the interactions between two species: prey and predators, serving as a cornerstone in mathematical biology and ecology by offering insights into natural population dynamics.

The model divides the total population into two distinct subpopulations: prey and predators. Prey are subject to predation at a rate δ, causing a decline in their numbers, and also experience natural mortality at rate γ. Predators, conversely, grow in number at a rate ε proportional to the prey population while suffering natural mortality at rate θ.

This interaction is mathematically expressed as:

$$\begin{cases} u'(t) = u(t)(\gamma - \delta v(t)), \\ v'(t) = -v(t)(\theta - \varepsilon u(t)), \\ u(0) = u_0, \quad v(0) = v_0. \end{cases}$$

Here, $u(t)$ and $v(t)$ denote prey and predator populations respectively. The term $\gamma - \delta v(t)$ represents the prey's net growth rate, balancing natural mortality and predation, while $-v(t)(\theta - \varepsilon u(t))$ accounts for the predator's net decline, reflecting natural death and dependence on prey availability.

Recent studies have advanced predator-prey modeling through diverse approaches. For example, Mehdi et al. [18,19] investigate chaotic bifurcation dynamics in predator-prey interactions with logistic growth and Holling type-II responses, analyzing stability and control mechanisms in discrete models with prey refuge effects, uncovering complex chaotic behaviors. Hammouch et al. [9] explore fractional-order predator-prey models incorporating Holling type-II functional responses, providing numerical simulations and detailed dynamic investigations using fractional calculus techniques. These works enrich our understanding of nonlinear and fractional dynamics in ecological systems.

Beyond ecology, the Lotka-Volterra system has been adapted to model various interactions, including epidemiological dynamics of infectious diseases such as measles, HIV, and COVID-19. In these cases, predator-prey dynamics analogously represent interactions between susceptible, infected, and recovered individuals, facilitating detailed analysis of disease spread and control measures.

The predator-prey model offers a foundational framework for understanding complex dynamical systems. By examining species interactions and parameter influences, researchers can develop new nonlinear dynamical models applicable across fields, from ecology to epidemiology. This framework underscores the power of mathematical modeling in capturing real-world complexities and provides valuable tools for predicting and managing dynamic behaviors across scientific disciplines.

Moreover, the integration of Artificial Intelligence (AI) introduces new dimensions to the analysis and modeling of complex systems. While nonlinear predator-prey models provide foundational insights into ecological dynamics, the advent of AI technologies brings advanced tools and methodologies that can significantly enhance our analytical capabilities.

Artificial Intelligence, a term first introduced by John McCarthy in 1956, has since evolved into a multifaceted field. Initially, AI required substantial processing power and time to develop, but today it encompasses several distinct types. Narrow AI, or Weak AI, represents the most common form, where systems are designed to perform specific tasks with high efficiency. For example, email spam detection and product recommendation systems are applications of Narrow AI. These systems excel within their designated tasks but lack broader cognitive abilities.

On the other hand, Artificial General Intelligence (AGI), also known as intelligent agents, is designed to replicate the full spectrum of human intellectual capabilities. AGI systems are capable of understanding and performing any cognitive task that a human can, showcasing remarkable adaptability and flexibility.

At the pinnacle of AI development is Artificial Superintelligence (ASI). This form of AI is envisioned to surpass human intelligence across all domains. Although still theoretical, ASI holds the promise of revolutionary advancements but also poses significant challenges due to its superior cognitive abilities.

John McCarthy's pioneering work laid the foundation for exploring various AI subfields, including machine learning, deep learning, and natural language

processing (NLP). Machine learning, a subset of AI, automates the learning process by enabling systems to improve from experience without explicit programming. Applications such as email spam filters and predictive analytics exemplify how machine learning can streamline and enhance diverse tasks.

Deep learning, a more specialized area within machine learning, utilizes artificial neural networks designed to simulate the human brain. This technology is particularly effective in complex tasks such as image and speech recognition. Deep learning algorithms continuously refine their performance by analyzing vast amounts of data, leading to significant advances in these areas.

In parallel, natural language processing (NLP) focuses on the ability of machines to understand and interact with human language. NLP drives innovations such as chatbots and language translation systems, relying on advanced language processing techniques to facilitate human-computer interaction.

By integrating AI methodologies with nonlinear dynamical systems such as predator-prey models, researchers can harness the power of machine learning and deep learning to develop more accurate and predictive models. This synergy enhances our ability to analyze and understand complex systems, paving the way for advances in both theoretical research and practical applications. For a visual representation of how these AI techniques are applied,

In addition to the advancements in artificial intelligence and neural networks, the integration of these technologies with partial differential equations (PDEs) represents a significant development in computational modeling. The application of neural networks to PDEs addresses some of the limitations of traditional interpolation models and iterative techniques, particularly in handling large-scale systems. This modern approach leverages the strengths of artificial neural networks (ANNs), which have been effectively utilized in regression and classification tasks [11,24].

The concept of fractional calculus (FC), introduced by Leibniz in the 17th century, has since evolved into a robust tool in various scientific domains. Initially a theoretical extension of integer-order calculus, fractional calculus is now extensively used across diverse fields. In physics, it models complex phenomena such as anomalous diffusion and quantum systems through fractional Schrödinger equations [6,14,15,45]. In biology, fractional calculus aids in predicting disease dynamics [1,13,16], while in engineering, it enhances control systems and signal processing [4]. Its versatility further extends to economics, finance, and medicine, showcasing broad applicability.

Several definitions of fractional derivatives have emerged, each offering unique perspectives and methodologies. These include the Riemann-Liouville fractional derivative [17,40], the Grünwald fractional derivative [8,21], the Hadamard derivative [42], and the Caputo fractional derivative [8,17]. Each contributes to the rich landscape of fractional calculus, providing valuable tools to address complex real-world problems.

This research builds upon these advancements, utilizing the strengths of artificial neural networks (ANNs) alongside fractional calculus to develop innovative solutions for dynamic systems. Previous works have demonstrated the effectiveness of fractional-order models in various contexts, such as the mathematical modeling and analysis of two-variable systems with non-integer order derivatives [23], fractional SEIR epidemic models [46], and multi-order models predicting COVID-19 outbreaks [10]. Additionally, fractional-order chaotic systems and delay differential equations have been studied using fractional iterative and synchronization methods [3,20].

The integration of artificial neural networks (ANNs) with fractional calculus offers a powerful framework for enhancing the accuracy and applicability of mathematical models across scientific and engineering domains. This combination effectively captures complex, memory-dependent dynamic behaviors inherent in many real-world systems.

In this paper, we propose a hybrid computational intelligence technique to solve fractional-order nonlinear predator-prey systems by combining artificial neural networks with a Genetic Algorithm-Interior Point Algorithm (GA-IPA) optimization. The ANN provides a flexible mathematical modeling structure, while the GA-IPA method optimizes the network parameters to achieve high precision. The novelty of our approach lies in the first application of this ANN-GA-IPA methodology to fractional-order dynamical systems, demonstrating improved computational efficiency and accuracy compared to conventional methods. By leveraging neural networks alongside metaheuristic optimization, this framework advances the modeling of complex ecological interactions and offers a scalable approach applicable to a broad range of nonlinear systems.

Recent developments in stochastic neural network solvers have shown remarkable success in addressing complex nonlinear and singular models. For instance, the stochastic Levenberg-Marquardt backpropagation neural network (LMBPNN) has been effectively applied to solve singular nonlinear sixth-order pantograph differential models combining pantograph and Emden-Fowler dynamics, with performance validated across training, validation, and testing phases [38]. Similarly, Bayesian-regularized radial basis neural networks (RBNN) have demonstrated high accuracy in modeling nonlinear malaria transmission dynamics [36], while radial basis deep neural networks (RBDNN), incorporating Bayesian regularization and implicit Runge-Kutta integration, have successfully captured predator-prey interactions [33]. Hybrid optimization approaches such as the radial basis scaled conjugate gradient neural network (RB-SCGNN) have been used to model the Zika virus dynamics, utilizing Runge-Kutta-generated data to ensure convergence and minimize error [37]. Additionally, stochastic LMBNN methods have been employed to solve fifth-order Emden-Fowler systems by partitioning datasets to reduce mean square error, achieving excellent agreement with reference solutions [31]. Collectively, these approaches highlight the versatility of stochastic solvers in managing singularities, multi-scale dynamics, and epidemiological compartmentalization, often outperforming traditional numerical methods through adaptive learning and robust regularization.

The application of computational intelligence in predator-prey system analysis has grown substantially. Combining ANNs with metaheuristic optimization algorithms has proven effective in solving complex nonlinear models with enhanced accuracy and efficiency. Such hybrid methods harness the adaptive learning capabilities of ANNs alongside the global search advantages of metaheuristics, making them well-suited for ecological modeling.

For example, Umar et al. [43] developed an intelligent computing framework integrating ANNs, genetic algorithms (GAs), and the interior-point algorithm (IPA) to analyze nonlinear predator-prey dynamics. Their approach was validated through statistical metrics including mean absolute error (MAE), root mean square error (RMSE), and Nash-Sutcliffe efficiency (NSE), with comparisons against traditional Adams numerical solvers. Similarly, Sabir et al. [28] introduced a Scaled Conjugate Gradient Neural Network (SCGNN) approach for fractional-order predator-prey models, effectively capturing memory-dependent biological dynamics and underscoring the potential of fractional calculus in ecological modeling, especially for systems with long-term dependencies.

Further enhancing computational efficiency, Umar et al. [44] developed a solver combining Morlet wavelet neural networks (MWNNs), genetic algorithms, and sequential quadratic programming (SQP). Their method achieved high accuracy in modeling predator-prey interactions, demonstrating the effectiveness of hybrid optimization techniques in ecological simulations. Likewise, Ruttanaprommarin et al. [26] investigated the use of Levenberg-Marquardt backpropagation in artificial neural networks to analyze delayed predator-prey models with Holling type-III functional responses. Their findings highlighted the robustness of this approach in handling nonlinearity and time delays, making it well-suited for realistic ecological systems.

Supervised learning techniques have been instrumental in advancing predator-prey modeling. Saeed et al. [39] utilized Levenberg-Marquardt backpropagation within supervised neural networks to solve nonlinear biological predator-prey systems. Their framework involved comprehensive training, validation, and testing phases, with performance evaluated through regression and correlation analyses. Recent innovations include specialized neural architectures such as the Gudermannian neural network (GNN), introduced by Alkaabi et al. [2]. Their hybrid methodology combined GNNs with genetic algorithms and interior-point optimization, achieving strong concordance with Runge-Kutta reference solutions. Additionally, Junsawang et al. [12] applied Levenberg-Marquardt backpropagation neural networks to solve a complex two-prey, one-predator delay differential system, showing excellent agreement with numerical benchmarks.

These computational techniques have also been extended to other biological systems. Sabir et al. [29] applied ANNs with Levenberg-Marquardt backpropagation to simulate influenza disease dynamics. Sanchez et al. [41] employed a hybrid artificial neural network-particle swarm optimization-interior point algorithm (ANN-PSO-IPA) framework for HIV infection modeling. Furthermore, Sabir et al. [27] developed a neuro-evolutionary method to solve multi-singular differential equations, illustrating the broad applicability of

these methods across complex nonlinear dynamic systems.

In this article, we extend the classical predator-prey model (Eq. (1)) by incorporating the fractional Caputo derivative, thereby introducing a more flexible and realistic framework that captures memory effects and non-local dynamics inherent in ecological interactions. Unlike traditional integer-order models, fractional-order formulations enable a nuanced representation of the complex temporal dependencies characteristic of predator-prey systems.

To advance our analysis, we employ artificial neural networks (ANNs) to estimate the population dynamics of both prey and predator species. This data-driven approach complements the fractional-order model by facilitating adaptive learning of the system's behavior, particularly valuable when obtaining precise analytical solutions is challenging. The neural network architecture is specifically designed to handle the nonlinearities induced by fractional dynamics, yielding robust and accurate numerical approximations.

Moreover, we develop a hybrid optimization framework that synergistically combines a genetic algorithm (GA) with an interior point algorithm (IPA) to efficiently calibrate model parameters and enhance computational performance. This GA-IPA hybrid leverages the global search strengths of genetic algorithms alongside the rapid local convergence properties of interior point methods, enabling precise and efficient parameter estimation even within complex, high-dimensional, and non-convex optimization landscapes.

The generalized fractional predator-prey system is formulated as:

$$\begin{cases} {}^{c}D^{\rho}u(t) = u(t)\big(\gamma^{\rho} - \delta^{\rho}v(t)\big), \\ {}^{c}D^{\rho}v(t) = -v(t)\big(\theta^{\rho} - \varepsilon^{\rho}u(t)\big), \\ u(0) = u_0, \quad v(0) = v_0. \end{cases} \tag{1}$$

The structure of this paper is as follows: Section 2 details the methodology employed to solve the nonlinear fractional predator-prey dynamic system (NFP-PDS). Section 3 presents the numerical results derived from this approach. Finally, the concluding section summarizes the main findings and discusses their significance in Section 4.

2 Design of the neural network

The neural network comprises H neurons in the input layer and a single output neuron. The weights in the input layer form an $H \times n$ matrix, while the weights in the second layer are represented by a vector of H elements. The output of the network is a vector denoted as $Y_{pred} = (u_{pred}(t), v_{pred}(t))$, as shown in Figure 1.

The outputs from the first layers are computed as:

$$\mathcal{Z}_u^{[1]} = W_u t + B_u, \quad \mathcal{Z}_v^{[1]} = W_v t + B_v$$

where W_u and W_v are the weight matrices, and B_u and B_v are the bias vectors. The predicted values for prey and predator are then given by:

$$u_{pred}(t) = \sum_{i=1}^{H} V_{u,i} A(\mathcal{Z}_{u,i}^{[1]}), \tag{2}$$

$$v_{pred}(t) = \sum_{i=1}^{H} V_{v,i} A(\mathcal{Z}_{v,i}^{[1]}), \tag{3}$$

where A is the activation function, specifically the sigmoid function:

$$A(x) = \frac{1}{1 + \exp(-x)}.$$

Thus, the equations become:

$$\begin{aligned} u_{pred}(t) &= \sum_{i=1}^{H} V_{u,i} \times \frac{1}{1 + \exp(-W_{u,i}t - B_{u,i})}, \\ v_{pred}(t) &= \sum_{i=1}^{H} V_{v,i} \times \frac{1}{1 + \exp(-W_{v,i}t - B_{v,i})}. \end{aligned} \tag{4}$$

The fractional derivatives of the predicted variables are computed as:

$$\begin{aligned} &{}^{c}D^{\rho}u_{pred}(t) \\ &= {}^{c}D^{\rho} \sum_{i=1}^{H} V_{u,i} \times \frac{1}{1 + \exp(-W_{u,i}t - B_{u,i})} \\ &= \frac{1}{\Gamma(1-\rho)} \sum_{i=1}^{H} V_{u,i} W_{u,i} \int_0^t (t-\tau)^{-\rho} A(W_{u,i}\tau \\ &\quad + B_{u,i})(1 - A(W_{u,i}\tau + B_{u,i}))d\tau, \end{aligned} \tag{5}$$

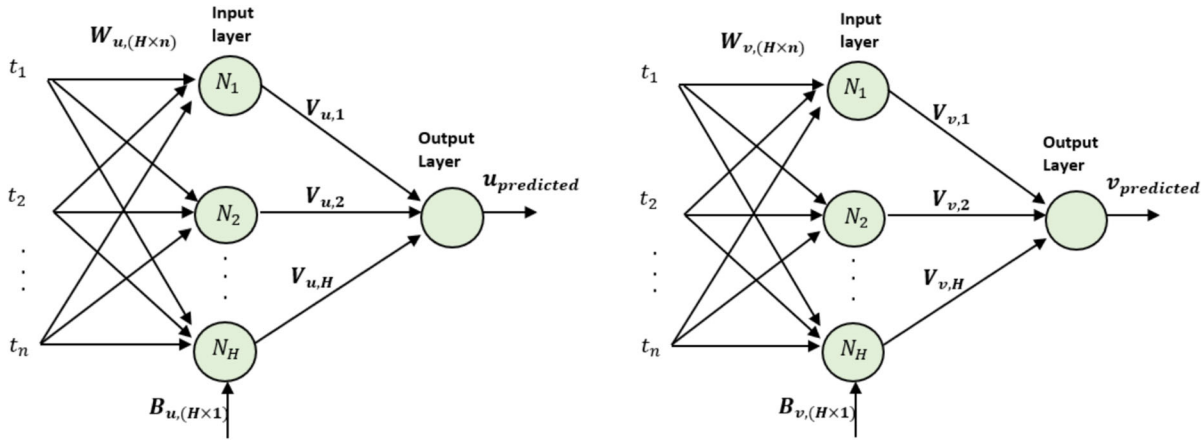

Fig. 1 A neural network architecture

$$
\begin{aligned}
&{}^{c}D^{\rho}v_{pred}(t)\\
&= {}^{c}D^{\rho}\sum_{i=1}^{H} V_{v,i} \times \frac{1}{1+\exp(-W_{v,i}t - B_{v,i})}\\
&= \frac{1}{\Gamma(1-\rho)}\sum_{i=1}^{H} V_{v,i}W_{v,i}\int_0^t (t-\tau)^{-\rho}A(W_{v,i}\tau\\
&\quad + B_{v,i})(1 - A(W_{v,i}\tau + B_{v,i}))d\tau.
\end{aligned}
\tag{6}
$$

To solve the fractional nonlinear predator-prey dynamical system, we first define the merit function. The merit function F_{Fit} is given by:

$$
F_{Fit} = F_{Fit-1} + F_{Fit-2} + F_{Fit-3}, \tag{7}
$$

where:

$$
\begin{aligned}
F_{Fit-1} &= \frac{1}{n}\sum_{i=1}^{n}\left({}^{c}D^{\rho}u_{pred,i} - u_{pred,i}(\gamma^{\rho} - \delta^{\rho}v_{pred,i})\right)^2,\\
F_{Fit-2} &= \frac{1}{n}\sum_{i=1}^{n}\left({}^{c}D^{\rho}v_{pred,i} + v_{pred,i}(\theta^{\rho} - \varepsilon^{\rho}u_{pred,i})\right)^2,\\
F_{Fit-3} &= \frac{1}{2}\left((u(0) - u_{pred,0})^2 + (v(0) - v_{pred,0})^2\right).
\end{aligned}
\tag{8}
$$

2.1 Measure of performance

This section provides a detailed analysis of the performance metrics for the nonlinear fractional predator-prey model, including Mean Square Error (MSE), Absolute Error (MAE), Theil Inequality Coefficient (TIC), and Error in Nash–Sutcliffe Efficiency (ENCE).

These metrics not only illustrate the trajectory of the method but also assess the accuracy of our approach in solving fractional nonlinear predator-prey differential equations. Then we express these measures in the following way,

The mean squared error (MSE) is defined as the average of the squared errors across all observations

$$
\begin{aligned}
MSE_u &= \frac{1}{n}\sum_{i=1}^{n}(u_i - u_{pred,i})^2,\\
MSE_v &= \frac{1}{n}\sum_{i=1}^{n}(v_i - v_{pred,i})^2,
\end{aligned}
\tag{9}
$$

Additionally, we define the mean absolute error in each instant t_j, for $j = 1, 2, \cdots, N$ by the following expressions

$$
\begin{aligned}
MAE_u &= \frac{1}{n}\sum_{i=1}^{n}|u_i - u_{pred,i}|,\\
MAE_v &= \frac{1}{n}\sum_{i=1}^{n}|v_i - v_{pred,i},|
\end{aligned}
\tag{10}
$$

The Theil Inequality Coefficient (Theil's U) measures a model's prediction accuracy by comparing its forecast errors to those of a naïve benchmark. The formal expression is as follows

$$
TIC_u = \frac{\sqrt{\frac{1}{n}\sum_{i=1}^{n}(u_i - u_{pred,i})^2}}{\sqrt{\frac{1}{n}\sum_{i=1}^{n}u_i^2}\sqrt{\frac{1}{n}\sum_{i=1}^{n}u_{pred,i}^2}},
$$

$$TIC_v = \frac{\sqrt{\frac{1}{n}\sum_{i=1}^{n}(v_i - v_{pred,i})^2}}{\sqrt{\frac{1}{n}\sum_{i=1}^{n} v_i^2}\sqrt{\frac{1}{n}\sum_{i=1}^{n} v_{pred,i}^2}}, \tag{11}$$

The Nash-Sutcliffe Efficiency (NSE) is a normalized statistic that measures the predictive ability of a hydrological or environmental model by comparing its performance to a benchmark simulation based on the mean of observed values

$$\begin{aligned} NES_u &= 1 - \frac{var(u_i - u_{pred,i})}{var(u_i)}, \\ NES_v &= 1 - \frac{var(v_i - v_{pred,i})}{var(v_i)}. \end{aligned} \tag{12}$$

The metrics MSE, MAE it measure the mean square error, and mean absolute error, respectively, associate to each state variable at all instants t_j, $j = 1, 2, ..., N$, as this values decrease as the predicted state are too close to the approximate state. The Thiel's Inequality Coefficient TIC is a normalized measure of the prediction error that ranges between 0 and 1. When TIC is too close to zero this is mean a best prediction of the state variable. While, when this value is close to 1 this indicate a completely inaccurate prediction. For NES is measure of the model's predictive power, ranging from $-\infty$ to 1 (1 is perfect prediction).

From a biological perspective, the mean squared error (MSE) quantifies the divergence between model predictions and empirical observations. Elevated MSE values may signal clinically relevant inaccuracies, whereas minimal MSE reflects close alignment with experimental or patient-derived data.

The mean absolute error (MAE) provides an intuitive measure of average deviation in natural units, offering practitioners direct insight into prediction reliability for individual cases.

For benchmarking, the normalized error score (NES) evaluates model performance against a naive reference (random chance). Superior NES values demonstrate the model's capacity to discern authentic biological patterns from stochastic variability.

Theil's inequality coefficient (TIC) serves as a normalized fidelity metric, where: 0 denotes perfect concordance with biological reality, and, 1 indicates biologically implausible predictions Models yielding lower TIC values exhibit stronger empirical validity (Fig. 2).

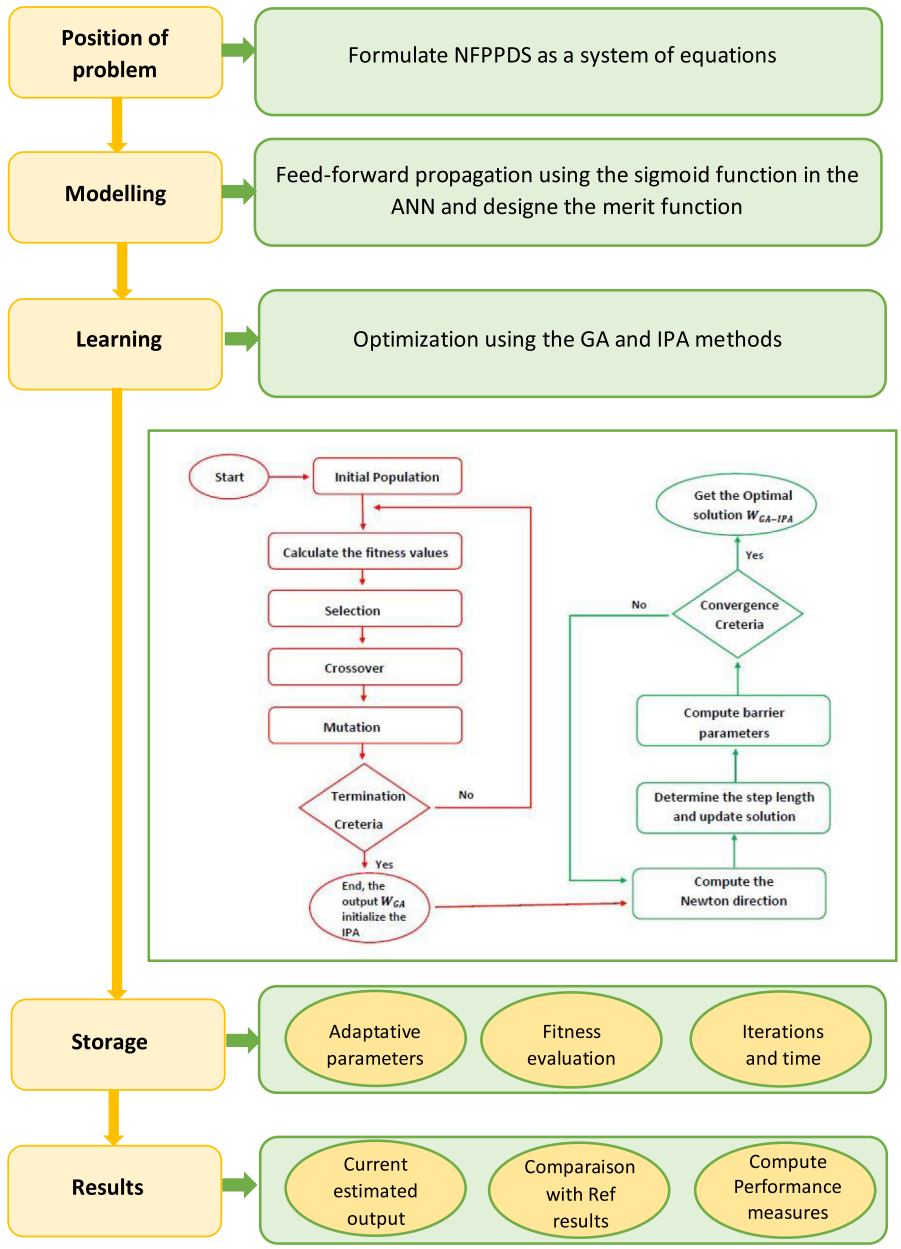

Fig. 2 Graphic representation of GA-IPA for solving the fractional nonlinear predator-prey dynamical system (NFPPDS)

GA Start :

Input: The chromosome signified with the same entries of the network as:

$\mathcal{C} = [\mathcal{C}_u, \mathcal{C}_v]$, for $\mathcal{C}_u = [V_u, w_u, B_u]$ and $\mathcal{C}_v = [V_v, w_v, B_v]$ where

$V_u = [V_{u,1}, V_{u,2}, \ldots, V_{u,H}], w_u = [w_{u,1}, w_{u,2}, \ldots, w_{u,H}], B_u = [B_{u,1}, B_{u,2}, \ldots, B_{u,H}]$

$V_v = [V_{v,1}, V_{v,2}, \ldots, V_{v,H}], w_v = [w_{v,1}, w_{v,2}, \ldots, w_{v,H}], B_v = [B_{v,1}, B_{v,2}, \ldots, B_{v,H}]$

Population: The set of chromosomes is written as: $P = [(\mathcal{C}_{u,1}, \mathcal{C}_{u,2}, \ldots, \mathcal{C}_{u,N}), (\mathcal{C}_{v,1}, \mathcal{C}_{v,2}, \ldots, \mathcal{C}_{v,N})]$

Where, $\mathcal{C}_{u,i} = (V_{u,i}, w_{u,i}, B_{u,i})$ and $\mathcal{C}_{v,i} = (V_{v,i}, w_{v,i}, B_{v,i})$

Output: The best GA values are assigned as $\mathcal{C}_{GA}$.

Initialization: **1.** Produce $\mathcal{C}$ vector using the real values to indicate a chromosome.

2. Adjust the $\mathcal{C}$ vector to form an initial : P

3. Regulate the generations and declarations values using gaoptimset

Fitness formulation: Obtained f_{Fit} for $\mathcal{C}$ in P using Eqs (8, 9)

Termining creteria: Execution of the scheme stop if: $f_{Fit} = 10^{-19}$, population size 200, max generations 200

Others: defaults values.

Store $\mathcal{C}_{GA}$ with time, f_{Fit}, generations, and current GA trials

End the GA process

Start the IPA process

Inputs: Primary weights are $\mathcal{C}_{GA}$

Outputs: GA-IPA is the weight vector $\mathcal{C}_{GA-IPA}$

Initialisation: $\mathcal{C}_{GA}$ is applied as an initial point

Termination creterias: [$f_{Fit} = 10^{-20}$], [iterations =891], [Maxfunctionevaluation=26000000], [TolFun=10^{-20}], [Tolx=10^{-22}],

While [Terminate],

Fitness Evaluation: To assess f_{Fit} of $\mathcal{C}$ for Eqs (8, 9)

Fine-tuning: 1. Apply **[fmincon]** routine,

2. Update the factors of $\mathcal{C}$ for each iteration of IPA and calculate f_{Fit} of enhanced $\mathcal{C}$ for Eqs (8, 9)

Store, store $\mathcal{C}_{GA-IPA}$, iterations , f_{Fit} , time, and function counts

End of IPA process

3 Numerical results

This section presents numerical results for the NFPPDS using the Neural Network and GA-IPA method to solve the system in equation (1). Due to the unavailability of exact solutions, we compare these results with reference outcomes based on the Adams-Bashforth fractional method [3,7]. The numerical results are provided for seven specific cases.

Case 1 : We consider the following fractional predator-prey dynamical system with the parameters, $\gamma = \frac{1}{3}, \delta = \frac{4}{3}, \theta = 1, \varepsilon = 1$ and the initial conditions $u_0 = 2$, and $v_0 = 4$ also the fractional order is fixed on $\rho = 0.8$

$$\begin{cases} {}^{c}D^{\rho}u(t) = u(t)((\frac{1}{3})^{0.8} - (\frac{4}{3})^{0.8} \times v(t)), \\ {}^{c}D^{\rho}v(t) = -v(t)(1 - u(t)), \\ u_0 = 2, \ v_0 = 4. \end{cases} \tag{13}$$

We apply the GA-IPA method with $H = 10$ neurons in the hidden layer and a time span of 5 units, using a step size of $h = 0.005$. This results in $n = \frac{\text{final time} - \text{initial time}}{h}$ nodes. Therefore, the functional objectif is written as follows:

$$F_{Fit} = F_{Fit-1} + F_{Fit-2} + F_{Fit-3}, \tag{14}$$

where,

$$\begin{aligned} F_{Fit-1} &= \frac{1}{n}\sum_{i=1}^{n}\left({}^{c}D^{0.8}u_{pred,i} - u_{pred,i}(\left(\frac{1}{3}\right)^{0.8}\right. \\ &\quad \left. - \left(\frac{4}{3}\right)^{0.7} v_{pred,i})\right)^2, \\ F_{Fit-2} &= \frac{1}{n}\sum_{i=1}^{n}\left({}^{c}D^{0.8}v_{pred,i} + v_{pred,i}(1 - u_{pred,i})\right)^2, \\ F_{Fit-3} &= \frac{1}{2}\left((2 - u_{pred,0})^2 + (4 - v_{pred,0})^2\right). \end{aligned} \tag{15}$$

Case 2 :In this case we consider the following fractional predator-prey dynamical system with the parameters, $\gamma = \frac{2}{3}$,$\delta = \frac{4}{3}$, $\theta = 1$, $\varepsilon = 1$ and the initial conditions $u_0 = 4$, and $v_0 = 6$ also the fractional order is fixed on $\rho = 0.7$

$$\begin{cases} {}^{c}D^{\rho}u(t) = u(t)(\left(\frac{2}{3}\right)^{0.8} - \left(\frac{4}{3}\right)^{0.7} \times v(t)), \\ {}^{c}D^{\rho}v(t) = -v(t)(1 - u(t)), \\ u_0 = 4, \ v_0 = 6. \end{cases} \tag{16}$$

We implement the GA-IPA method with $H = 10$ neurons in the hidden layer over a 5-unit time span, utilizing a step size of $h = 0.005$. Consequently, the number of nodes is given by $n = \frac{\text{final time}-\text{initial time}}{h}$. Therefore, the functional objectif is written as follows:

$$F_{Fit} = F_{Fit-1} + F_{Fit-2} + F_{Fit-3}, \tag{17}$$

where,

$$\begin{aligned} F_{Fit-1} &= \frac{1}{n}\sum_{i=1}^{n}\left({}^{c}D^{0.8}u_{pred,i} - u_{pred,i}\left(\left(\frac{2}{3}\right)^{0.8} - \left(\frac{4}{3}\right)^{0.8} v_{pred,i}\right)\right)^2, \\ F_{Fit-2} &= \frac{1}{n}\sum_{i=1}^{n}\left({}^{c}D^{0.8}v_{pred,i} + v_{pred,i}(1 - u_{pred,i})\right)^2, \\ F_{Fit-3} &= \frac{1}{2}\left((4 - u_{pred,0})^2 + (6 - v_{pred,0})^2\right). \end{aligned} \tag{18}$$

Case 3 : Consider the following fractional predator-prey dynamical system with parameters $\gamma = 1$, $\delta = \frac{4}{3}$, $\theta = 1$, $\varepsilon = 1$, and initial conditions $u_0 = 3$ and $v_0 = 9$. The fractional order is fixed at $\rho = 0.8$.

$$\begin{cases} {}^{c}D^{\rho}u(t) = u(t)(1 - (\frac{4}{3})^{0.8} \times v(t)), \\ {}^{c}D^{\rho}v(t) = -v(t)(1 - u(t)), \\ u_0 = 3, \ v_0 = 9. \end{cases} \tag{19}$$

As in the previous case, we apply the GA-IPA method with $H = 10$ neurons in the hidden layer over a 5-unit time span, using a step size of $h = 0.005$. This results in $n = \frac{\text{final time}-\text{initial time}}{h}$ nodes. Therefore, the functional objectif is written as follows:

$$F_{Fit} = F_{Fit-1} + F_{Fit-2} + F_{Fit-3}, \tag{20}$$

where,

$$\begin{aligned} F_{Fit-1} &= \frac{1}{n}\sum_{i=1}^{n}\left({}^{c}D^{0.8}u_{pred,i} - u_{pred,i}\left(1 - \left(\frac{4}{3}\right)^{0.8} v_{pred,i}\right)\right)^2, \\ F_{Fit-2} &= \frac{1}{n}\sum_{i=1}^{n}\left({}^{c}D^{0.8}v_{pred,i} + v_{pred,i}(1 - u_{pred,i})\right)^2, \\ F_{Fit-3} &= \frac{1}{2}\left((3 - u_{pred,0})^2 + (9 - v_{pred,0})^2\right). \end{aligned} \tag{21}$$

Table 1 presents the predicted states of the predator-prey system for Cases 1, 2, and 3 at time instants $t = 0.0, 0.5, 1.0, 1.5, 2.0, 2.5, 3.0, 3.5, 4.0, 4.5,$ and 5.0. The solutions demonstrate the temporal evolution of both predator (v_{pred}) and prey (u_{pred}) populations in each case 1, 2, and 3.

Figures 3, 4, 5, 6, 7, 8, 9, 10, 11, 12, 13, 14, 15, 16, and 17 display the numerical results for these cases, providing a comprehensive comparison of the optimization techniques under investigation.

Figures 3 and 4 show fitness values derived with the genetic algorithm (GA) and the interior point method (IPA), illustrating their distinct convergence characteristics. For example, Figure 3 shows the final fitness values for the three test cases as 0.83, 1.63, and 0.3 when employing the genetic algorithm. While these results indicate the GA's ability to explore a large search field, they also reveal areas for improvement.

To improve precision, the interior point algorithm (IPA) was set up with the GA answers as starting points. The hybrid technique improved outcomes dramatically, with the IPA obtaining fitness values of 0.15×10^{-4} for case 1, 10^{-4} for case 2, and 2.5×10^{-5} for case 3. The significant reduction in fitness values demonstrates the IPA's efficacy in fine-tuning solutions near optimal regions.

Figure 5 shows a histogram of fitness values for the three scenarios under examination. Subfigure 5a shows that most fitness values cluster around 325, generating a clear peak in the distribution. Beyond this peak, frequency drops sharply, implying that numbers much higher or lower than 325 are rare. The overlay red curve, which represents a smoothed density estimate, accentuates the data's central tendency while verifying that the distribution is unimodal and has a tight concen-

Table 1 Series solutions of predicted states in cases 1, 2, and 3

Time	Case 1		Case 2		Case 3	
	u_{pred}	v_{pred}	u_{pred}	v_{pred}	u_{pred}	v_{pred}
0.0	2	3.9998	3.9994	5.9997	2.9999	8.9998
0.5	2.3389	0.8542	3.3864	0.88785	0.86963	2.8679
1.0	3.1466	0.34711	4.4037	0.35676	0.80119	1.7517
1.5	4.2681	0.17464	5.9342	0.17904	0.86481	1.1918
2.0	5.7961	0.10136	8.0108	0.10545	1.0019	0.85797
2.5	7.8626	0.059281	10.847	0.063691	1.2003	0.6355
3.0	10.652	0.035008	14.669	0.037766	1.4702	0.4757
3.5	14.421	0.022141	19.842	0.023735	1.8368	0.3564
4.0	19.516	0.015781	26.832	0.016945	2.3374	0.26591
4.5	26.397	0.012787	36.282	0.013881	3.0189	0.19693
5.0	35.691	0.011422	49.051	0.012558	3.9313	0.14435

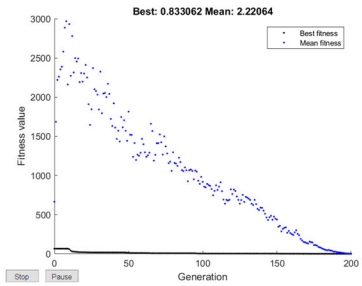

(a) **case 1** : values via GA.

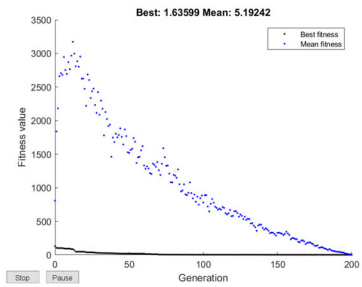

(b) **case 2** : Fitness values via GA.

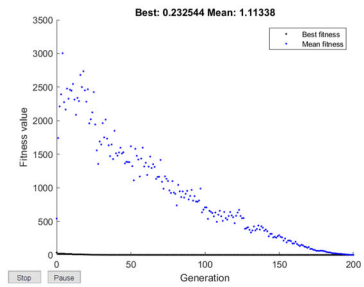

(c) **case 3** : Fitness values via GA.

Fig. 3 The fitness value via the GA method

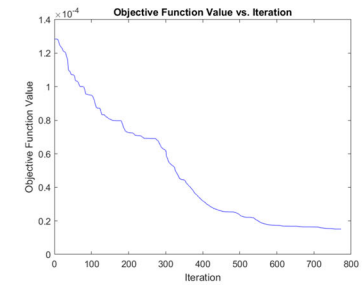

(a) **case 1** : Fitness values via IPA.

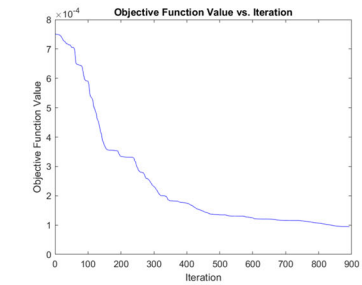

(b) **case 2** : Fitness values via IPA.

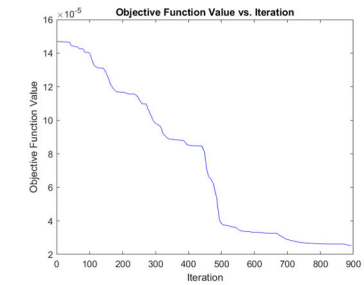

(c) **case 3** : Fitness values via IPA.

Fig. 4 The fitness value via the IPA method

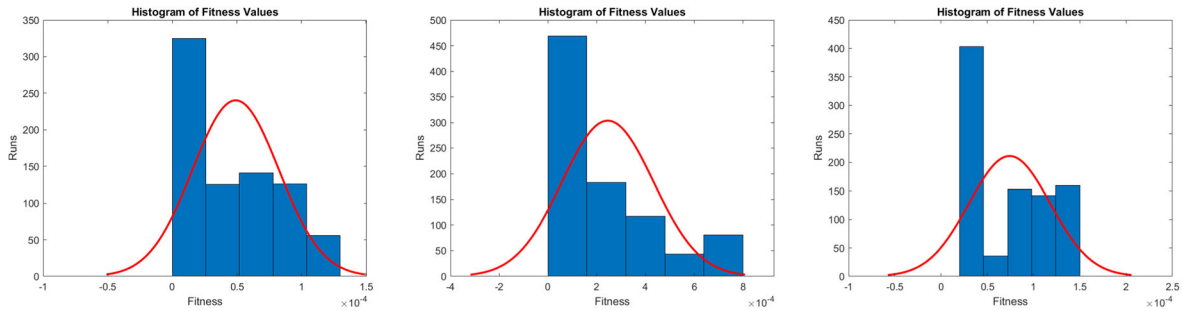

(a) **case 1** : Histogram values. (b) **case 2** : Histogram values. (c) **case 3** : Histogram values.

Fig. 5 Histogram plots of the fitness values in the cases 1, 2, and 3

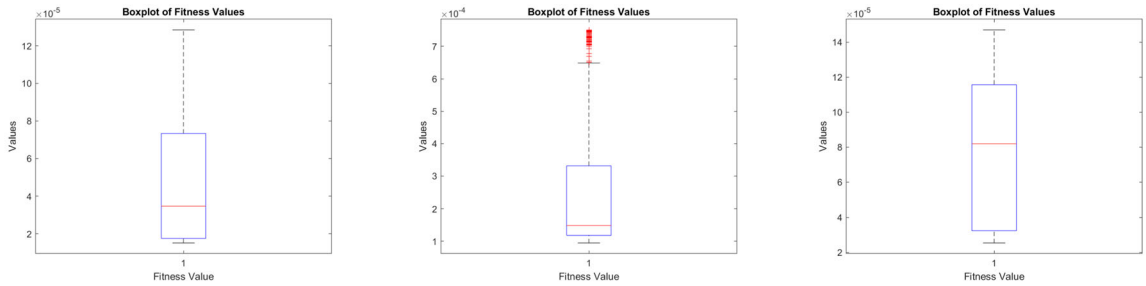

(a) **case 1** : Boxplot of fitness values. (b) **case 2** : Boxplot of fitness values. (c) **case 3** : Boxplot of fitness values.

Fig. 6 Boxplots of the fitness values in the cases 1, 2, and 3

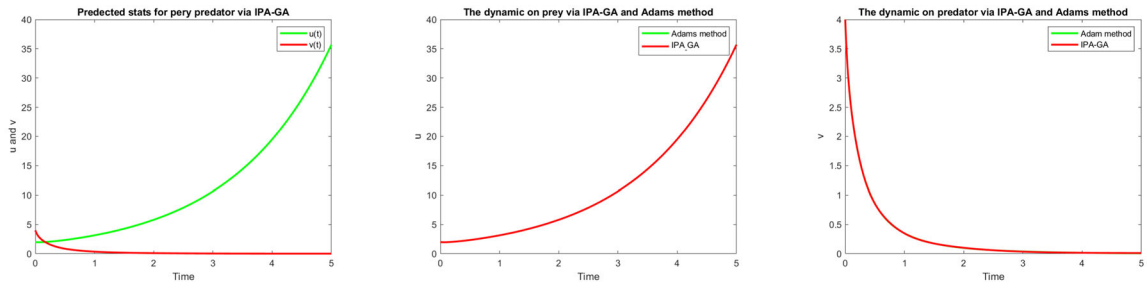

(a) **Case 1** : States variables via GA-IPA method (b) **Case 1** : The states variable $u(t)$ via GA-IPA method. (c) **Case 1** : The states variable $u(t)$ via GA-IPA method.

Fig. 7 States variables via GA-IPA method in case 1

tration around the mean. Subfigures 5b and 5c show similar trends for other fitness function settings, confirming the constancy of this tendency across several experimental setups.

Figure 6 shows boxplots summarizing the merit function's distribution, providing a detailed picture of its statistical characteristics. The subfigure 6a depicts the fitness values' central tendency (median) and dispersion (interquartile range, whiskers). Notably, the existence of many outliers above the upper whisker indicates that, while the majority of solutions converge within a narrow range, a fraction obtains much higher fitness values. The median 50% of the data (interquar-

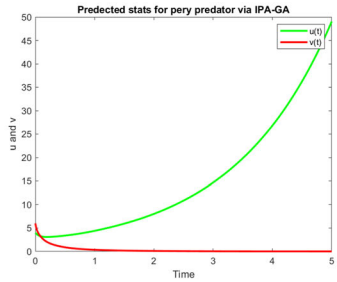

(a) **case 2** : States variables via GA-IPA method.

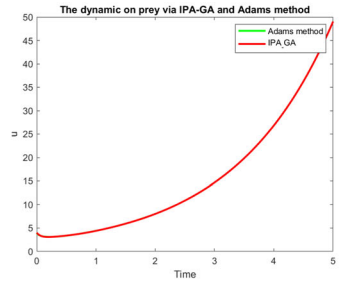

(b) **case 2** : State variable $u(t)$ via GA-IPA method.

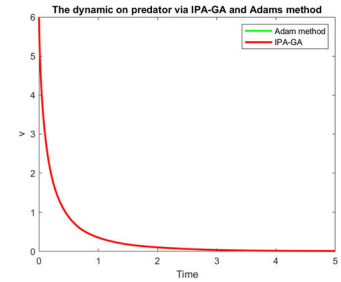

(c) **case 2** : State variable $v(t)$ via GA-IPA method.

Fig. 8 Boxplots of the fitness values in the cases 1, 2, and 3

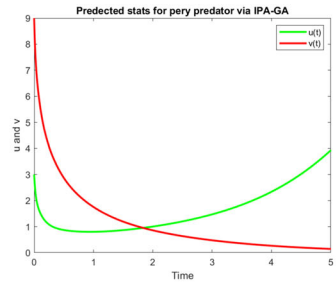

(a) **case 3** : States variables via GA-IPA method.

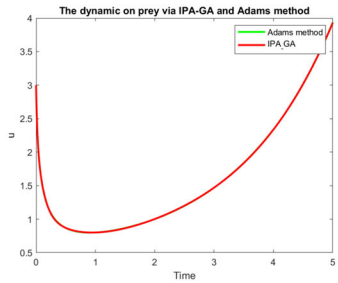

(b) **case 3** : States variables via $u(t)$ GA-IPA method.

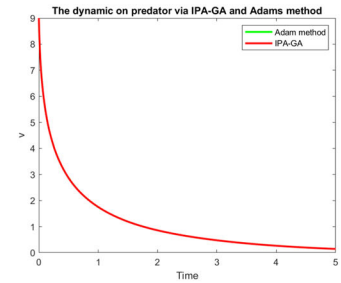

(c) **case 3** : State variable $v(t)$ via GA-IPA method.

Fig. 9 States variables via GA-IPA method in case 1

Fig. 10 The absolute error between the GA-IPA method and the Adams approach for the state $u(t)$

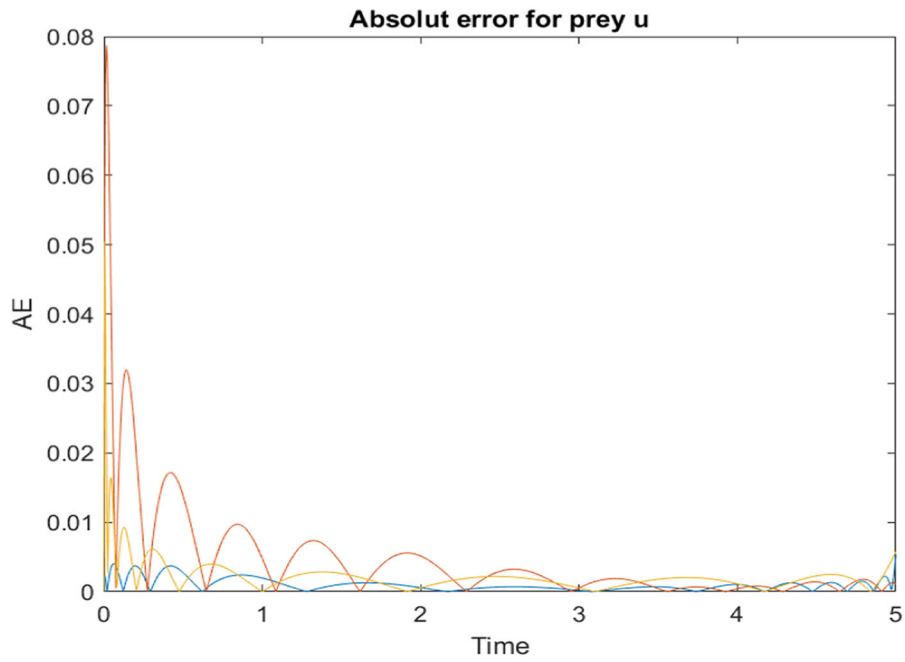

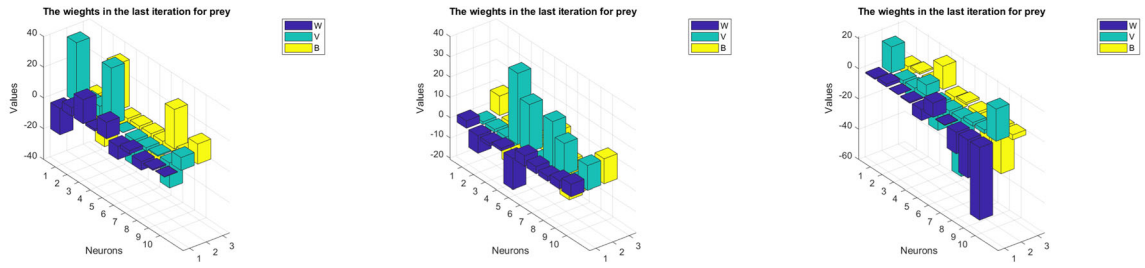

(a) **case 1** : Weights vectors for pery $u(t)$.

(b) **case 2** : Weights vectors for pery $u(t)$.

(c) **case 3** : Weights vectors for pery $u(t)$.

Fig. 11 The 3D-Histogram shows the values of the weights vectors prey stat in each case 1,2 and 3

Fig. 12 The absolute error between the GA-IPA method and the Adams approach for the state $v(t)$

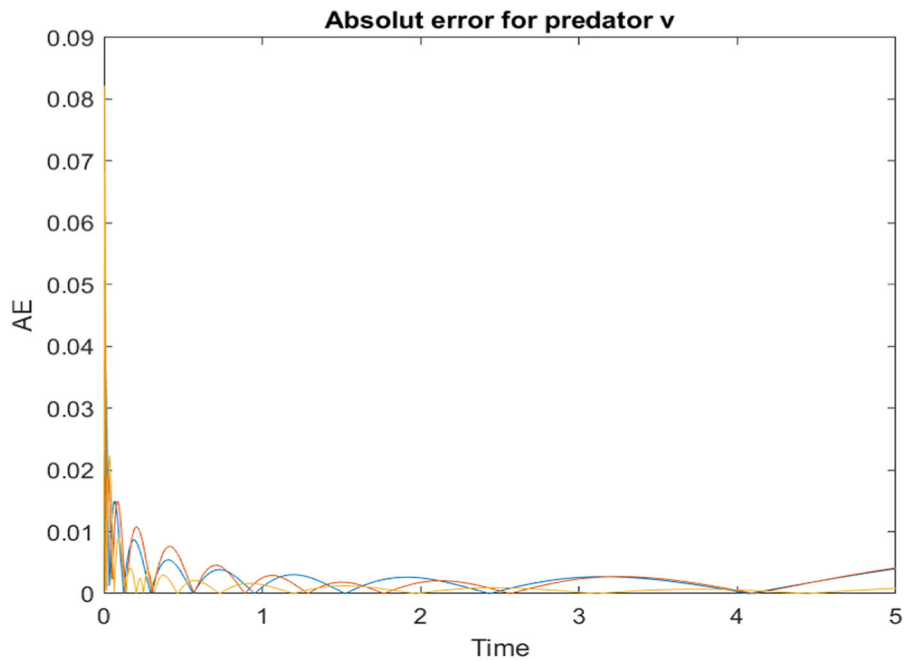

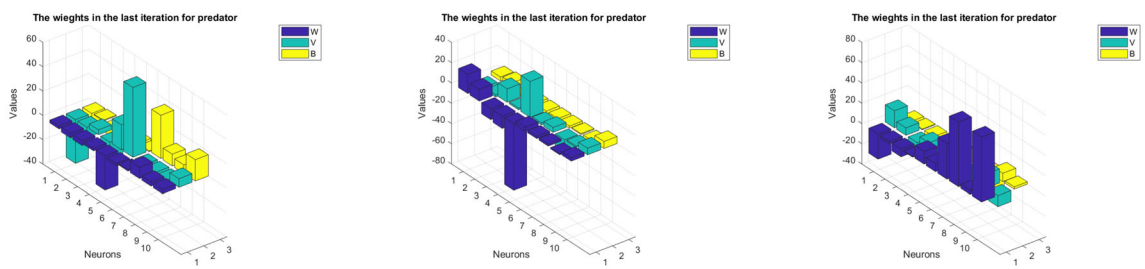

(a) **case 1** : Weights vectors for perdator $v(t)$.

(b) **case 2** : Weights vectors for perdator $v(t)$.

(c) **case 3** : Weights vectors for perdator $v(t)$.

Fig. 13 The 3D-Histogram shows the values of the weights vectors prey stat in each case 1,2 and 3

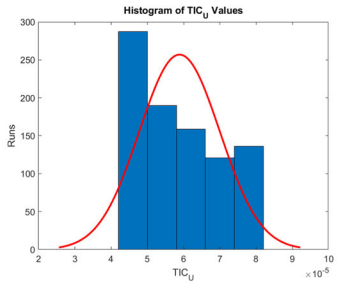

(a) **case 1** : Histogram of TIC values of prey $u(t)$.

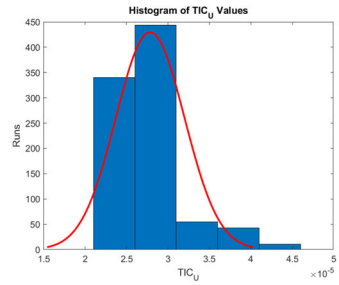

(b) **case 2** : Histogram of TIC values of prey $u(t)$.

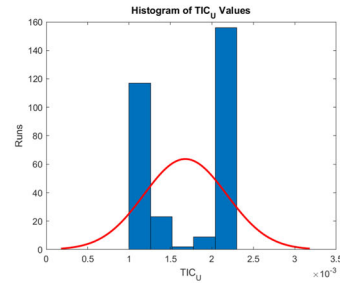

(c) **case 3** : Histogram of TIC values of prey $u(t)$.

Fig. 14 Histogram of TIC values of prey $u(t)$ in the case 1, 2 and 3

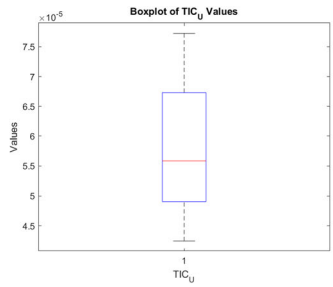

(a) **case 1** : Boxplot of TIC values of prey $u(t)$.

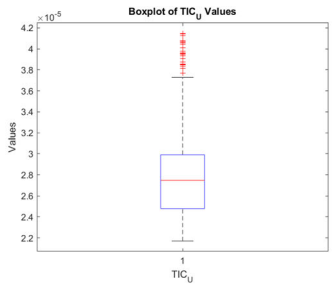

(b) **case 2** : Boxplot of TIC values of prey $u(t)$.

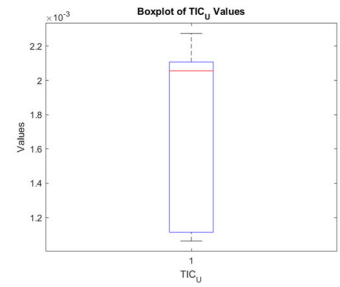

(c) **case 3** : Boxplot of TIC values of prey $u(t)$.

Fig. 15 Boxplot of TIC values of prey $u(t)$ in the case 1,2 and 3

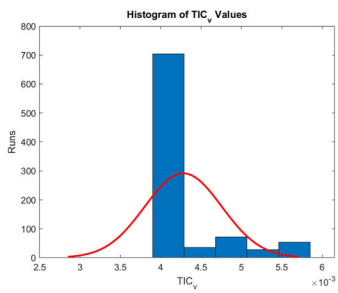

(a) **case 1** : Histogram of TIC values of predator $v(t)$.

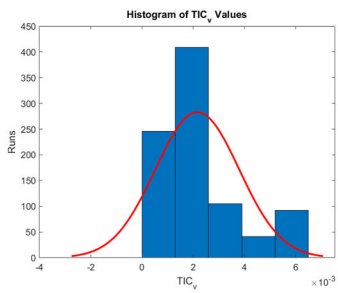

(b) **case 2** : Histogram of TIC values of predator $v(t)$.

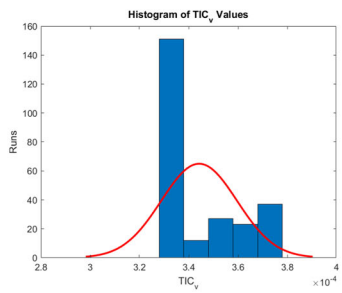

(c) **case 3** : Histogram of TIC values of predator $v(t)$.

Fig. 16 Histogram of TIC values of predator $v(t)$ in the case 1,2 and 3

tile range) ranges from 10^{-4} to 3×10^{-4}, suggesting a minimal variability for the majority of observations.

Further comparative analysis is provided in Figures 7, 8, and 9, which statistically contrast the performance of the Genetic Algorithm-Interior Point Algorithm (GA-IPA) hybrid method against the conventional Adams method in modeling a fractional predator-prey dynamical system. The absolute errors between these two approaches, visualized in Figures 10 and 12, reveal that the GA-IPA method consistently achieves lower error magnitudes, underscoring its superior precision.

Figures 14–17 demonstrate the Theil Inequality Coefficient (TIC) as an additional validation of the GA-

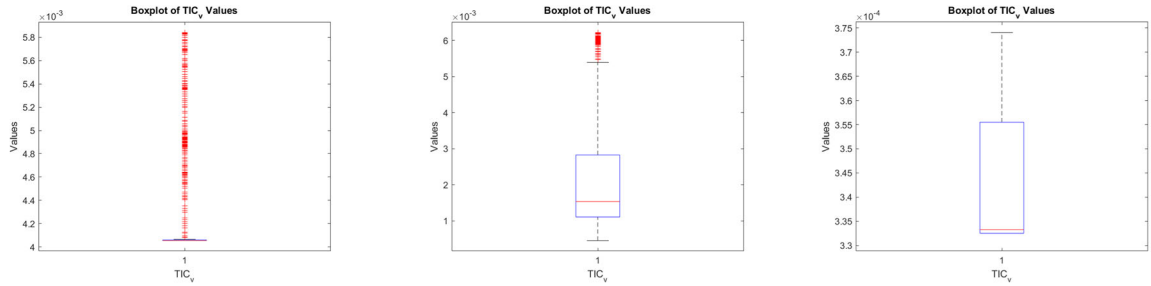

(a) **case 1** : Boxplot of TIC values of predator $v(t)$.

(b) **case 2** : Boxplot of TIC values of predator $v(t)$.

(c) **case 3** : Boxplot of TIC values of predator $v(t)$.

Fig. 17 Boxplot of TIC values of predator $v(t)$ in the case 1,2 and 3

Table 2 Series solutions of predicted states in cases 4, 5, and 6

Time	Case 4		Case 5		Case 6	
	u_{pred}	v_{pred}	u_{pred}	v_{pred}	u_{pred}	v_{pred}
0.0	1.9999	3.9999	3.9998	5.9994	2.9998	8.9998
0.5	0.565	2.0009	0.98258	2.2031	0.43713	3.6503
1.0	0.50905	1.4927	0.89446	1.6024	0.37581	2.6928
1.5	0.49945	1.2097	0.91248	1.2848	0.36836	2.1796
2.0	0.51114	1.0298	0.95934	1.0603	0.37459	1.8331
2.5	0.53622	0.89696	1.0231	0.89128	0.38543	1.5823
3.0	0.56967	0.79316	1.1036	0.76271	0.39914	1.3972
3.5	0.60831	0.71143	1.2031	0.66487	0.41572	1.255
4.0	0.65011	0.6475	1.3244	0.59049	0.43556	1.1383
4.5	0.69377	0.59789	1.4706	0.53397	0.45926	1.0357
5.0	0.73845	0.55966	1.6454	0.49106	0.48753	0.93998

IPA method's efficacy. The TIC values, which define prediction accuracy, are consistently near zero throughout all examined states (e.g., $u(t)$ and $v(t)$. Figure 14 shows that the TIC for state $u(t)$ is within a limited range of 1.1×10^{-3} to 2.1×10^{-3}, indicating the method's reliability. These findings imply that the GA-IPA method beats the Adams method in terms of precision and robustness, indicating that it is a promising tool for analyzing complicated dynamical systems.

Figures 7, 8, and 9 present the behavior of the state variables u and v in comparison with the Adams method, using the same fractional order $\rho = 0.7$ in the three cases 1, 2, and 3 respectively.

The weights vector that's gives those optimal resualts are showed in the histogram figure 11

The weight vector that yields these optimal results is shown in the histogram in Figure 13.

Case 4 : Now we consider the following fractional predator-prey dynamical system with the parameters, $\gamma = \frac{2}{3}$,$\delta = \frac{4}{3}$, $\theta = 1$, $\varepsilon = 0.2$ and the initial conditions $u_0 = 2$, and $v_0 = 4$ also the fractional order is fixed on $\rho = 0.65$

$$\begin{cases} {}^{c}D^{\rho}u(t) = u(t)((\frac{2}{3})^{0.65} - (\frac{4}{3})^{0.65} \times v(t)), \\ {}^{c}D^{\rho}v(t) = -v(t)(1 - 0.2^{0.65}u(t)), \\ u_0 = 2,\ v_0 = 4. \end{cases} \tag{22}$$

We apply the GA-IPA method with $H = 10$ neurons in the hidden layer and a time span of 5 units with a step size of $h = 0.005$. This results in $n = \frac{\text{final time}-\text{initial time}}{h}$ nodes. Therefore, the functional objectif is written as follows:

$$F_{Fit} = F_{Fit-1} + F_{Fit-2} + F_{Fit-3}, \tag{23}$$

where,

$$\begin{aligned}
F_{Fit-1} &= \frac{1}{n}\sum_{i=1}^{n}\left({}^{c}D^{0.65}u_{pred,i} - u_{pred,i}\left(\left(\frac{2}{3}\right)^{0.65} - \left(\frac{4}{3}\right)^{0.65} v_{pred,i}\right)\right)^2,\\
F_{Fit-2} &= \frac{1}{n}\sum_{i=1}^{n}\left({}^{c}D^{0.65}v_{pred,i} + v_{pred,i} \times \left(1 - 0.2^{0.65}u_{pred,i}\right)\right)^2,\\
F_{Fit-3} &= \frac{1}{2}\left((2-u_{pred,0})^2 + (4-v_{pred,0})^2\right).
\end{aligned} \tag{24}$$

Case 5 : Now we consider the following fractional predator-prey dynamical system with the parameters, $\gamma = \frac{2}{3}$,$\delta = \frac{4}{3}$, $\theta = 1$, $\varepsilon = 0.65$ and the initial conditions $u_0 = 4$, and $v_0 = 6$ also the fractional order is fixed on $\rho = 0.65$

$$\begin{cases}
{}^{c}D^{\rho}u(t) = u(t)((\frac{2}{3})^{0.65} - (\frac{4}{3})^{0.65} \times v(t)),\\
{}^{c}D^{\rho}v(t) = -v(t)(1 - 0.65^{0.65}u(t)),\\
u_0 = 4,\ v_0 = 6.
\end{cases} \tag{25}$$

We use the GA-IPA method with $H = 10$ neurons in the hidden layer, a time span of 5 units, and a step size of $h = 0.005$. This configuration results in $n = \frac{\text{final time}-\text{initial time}}{h}$ nodes. Therefore, the functional objectif is written as follows:

$$F_{Fit} = F_{Fit-1} + F_{Fit-2} + F_{Fit-3}, \tag{26}$$

where,

$$\begin{aligned}
F_{Fit-1} &= \frac{1}{n}\sum_{i=1}^{n}\left({}^{c}D^{0.65}u_{pred,i} - u_{pred,i} \times \left(\left(\frac{2}{3}\right)^{0.65} - \left(\frac{4}{3}\right)^{0.65} v_{pred,i}\right)\right)^2,\\
F_{Fit-2} &= \frac{1}{n}\sum_{i=1}^{n}\left({}^{c}D^{0.65}v_{pred,i} + v_{pred,i}(1 - 0.65^{0.65}u_{pred,i})\right)^2,\\
F_{Fit-3} &= \frac{1}{2}\left((4-u_{pred,0})^2 + (6-v_{pred,0})^2\right).
\end{aligned} \tag{27}$$

Case 6 : We now examine the fractional predator-prey dynamical system with the parameters $\gamma = \frac{2}{3}$, $\delta = \frac{4}{3}$, $\theta = 1$, $\varepsilon = 1$, and initial conditions $u_0 = 3$ and $v_0 = 9$. The fractional order is set at $\rho = 0.65$.

$$\begin{cases}
{}^{c}D^{\rho}u(t) = u(t)((\frac{2}{3})^{0.65} - (\frac{4}{3})^{0.65} \times v(t)),\\
{}^{c}D^{\rho}v(t) = -v(t)(1 - u(t)),\\
u_0 = 3,\ v_0 = 9.
\end{cases} \tag{28}$$

We use the GA-IPA method with $H = 10$ neurons in the hidden layer, over a 5-unit time span with a step size of $h = 0.005$. This setup results in $n = \frac{\text{final time}-\text{initial time}}{h}$ nodes. Therefore, the functional objectif is written as follows:

$$F_{Fit} = F_{Fit-1} + F_{Fit-2} + F_{Fit-3}, \tag{29}$$

where,

$$\begin{aligned}
F_{Fit-1} &= \frac{1}{n}\sum_{i=1}^{n}\left({}^{c}D^{0.65}u_{pred,i} - u_{pred,i}\left(\left(\frac{2}{3}\right)^{0.65} - \left(\frac{4}{3}\right)^{0.65} v_{pred,i}\right)\right)^2,\\
F_{Fit-2} &= \frac{1}{n}\sum_{i=1}^{n}\left({}^{c}D^{0.65}v_{pred,i} + v_{pred,i}\left(1 - u_{pred,i}\right)\right)^2,\\
F_{Fit-3} &= \frac{1}{2}\left((3-u_{pred,0})^2 + (9-v_{pred,0})^2\right).
\end{aligned} \tag{30}$$

Table 2 presents the predicted states of the predator-prey system for Cases 4, 5, and 6 at time instants $t = 0.0, 0.5, 1.0, 1.5, 2.0, 2.5, 3.0, 3.5, 4.0, 4.5,$ and 5.0. The solutions demonstrate the temporal evolution of both predator (v_{pred}) and prey (u_{pred}) populations in each case 4, 5, and 6.

Figures 18 through 32 show the efficiency of the hybrid Genetic Algorithm-Interior Point Algorithm (GA-IPA) technique. Figures 18 and 19 show the fitness values obtained from the genetic algorithm and the interior point approach, respectively. IPA achieves much lower fitness values (0.4×10^{-4} for case 4) than GA alone (0.23 for case 4), showcasing IPA's refinement capacity when initiated by GA solutions. This significant improvement implies that the hybrid strategy effectively combines GA's global search and IPA's local convergence (Fig. 23).

Figure 20 shows a histogram of fitness values across three scenarios, with a concentration around 550 and decreasing frequency beyond this point. The adjacent red curve depicts the distribution pattern, which has a distinct center tendency. Figure 21 analyzes these results through boxplots of the merit function. The medianks in each case is concetrated between 1.2×10^{-4} in case 4 to 0.7×10^{-4} in case 6. These narrow boundaries suggest consistent performance with low variability among runs.

The method's application to fractional predator-prey systems is shown in Figs. 22–24, comparing GA-IPA results with the Adams method. The absolute errors between these approaches, depicted in Figs. 25 and 27, decrease below 10^{-3} over time. This convergence demonstrates the hybrid method's ability to accurately capture system dynamics, particularly for challenging fractional-order systems where traditional methods may struggle.

Figures 29–32 show the Theil Inequality Coefficient (TIC) study, which analyzes method agreement quantitatively. Boxplots and histograms indicate TIC values continuously near to 0, with precise ranges of 1×10^{-3} to 10.5×10^{-3} for state $u(t)$ (Fig. 30a). Figures 30b, 30c, and 32a –32c show similar findings for other states, confirming the correctness of the technique across all system components. The narrow distributions of TIC values suggest consistent performance with little variation from reference solutions (Fig. 31).

These findings show that the GA-IPA hybrid technique successfully solves fractional-order dynamical systems by combining the strengths of global optimization and local refining. The consistently low fitness values, narrow error distributions, and low TIC coefficients indicate that the technique is both accurate and reliable. The method's performance across several test scenarios demonstrates robustness, giving it a promising alternative to traditional methodologies for complicated nonlinear systems.

The weights vector that's gives those optimal resualts are showed in the histogram Fig. 26

The weights vector that's gives those optimal resualts are showed in the histogram Fig. 28

Case 7 : In this case, we show the effect of the fractional order on the dynamics of NFPPDS. Then, for this purpose, we varied the fractional order ρ, while the other parameters are fixed in the values $\gamma = 2/3, \delta = 4/3, \theta = 1$, and $\varepsilon = 1$. Figures 33b and 34b show the population dynamics of predator and prey species using our fractional-order model. These findings show how the fractional Caputo derivative captures the complicated relationships of the two populations. Figures 33a and 34a provide a comparison of the typical Adams-Bashforth technique answers. Interestingly, we find that both techniques predict almost identical behavioral patterns for predator and prey populations throughout fractional orders. This extraordinary consistency implies an intrinsic symmetry in their ecological interactions that remains regardless of the derivative order used in the modeling approach.

The use of fractional calculus, particularly the Caputo derivative framework, offers numerous important advantages over typical integer-order models in ecological modeling. First, the fractional approach naturally incorporates memory effects, allowing the model to account for how past population conditions influence current dynamics. This is especially useful in predator-prey systems, where past population densities, seasonal fluctuations, and cumulative environmental influences all play important roles in determining contemporary interactions. The non-local nature of fractional operators allows the model to capture long-term dependencies that traditional models sometimes ignore.

Recent studies on predator-prey systems have predominantly focused on classical integer-order dynamics, neglecting the nuanced memory-dependent and non-local interactions captured by fractional calculus (see, [2,26,29]). For example, the study in [2] presents Gudermannian Neural Networks (GNNs) for solving a nonlinear biological predator-prey system, optimized using a hybrid genetic algorithm-interior point algorithm (GA-IPA). Six variants of the model were tested, and the results confirmed the scheme's accuracy. The

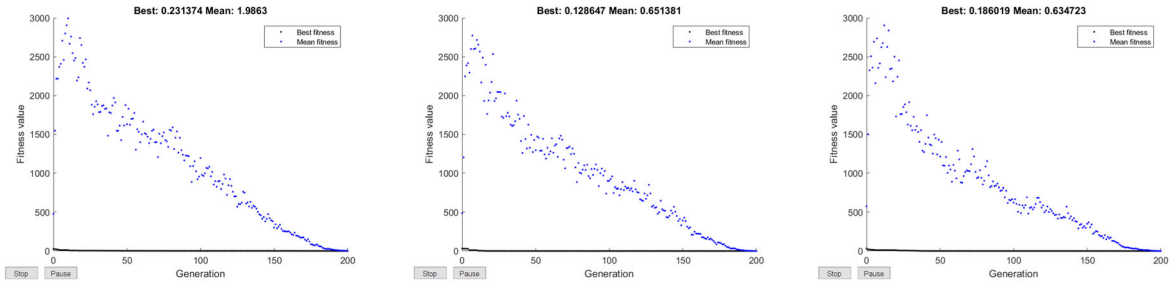

(a) **Case 4** : Fitness values via GA. (b) **Case 5** : Fitness values via GA. (c) **Case 6** : Fitness values via GA.

Fig. 18 The fitness value via the hybrid GA method

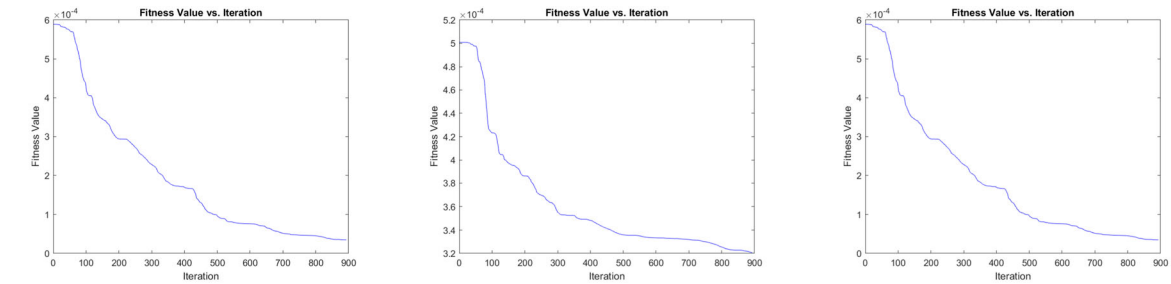

(a) **Case 4** : Fitness values via IPA. (b) **Case 5** : Fitness values via IPA. (c) **Case 6** : Fitness values via IPA.

Fig. 19 The fitness value via the hybrid IPA method

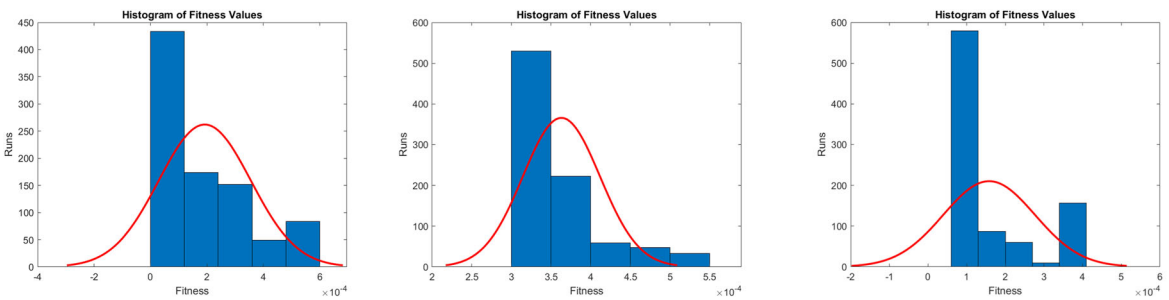

(a) **case 4** : Histogram value. (b) **case 5** : Histogram value. (c) **case 6** : Histogram values in case 3.

Fig. 20 Histogram plots of the fitness values in the cases 4, 5, and 6

method's reliability was demonstrated by low Absolute Error values. Statistical performance was assessed using Min, and Median, with small error values validating the method's precision. Further validation was conducted through Fit, TIC, and ENSE, confirming high accuracy across multiple trials. In the field of fractional order predator-prey, the paper [28] investigate an infection-based fractional-order nonlinear predator-prey system using stochastic scaled conjugate gradient neural networks (SCGNNs). The model was tested with three fractional-order values and validated against the Adams-Bashforth-Moulton method. The SCGNNs demonstrated high accuracy, reliability, and computational efficiency, confirming the method's robustness

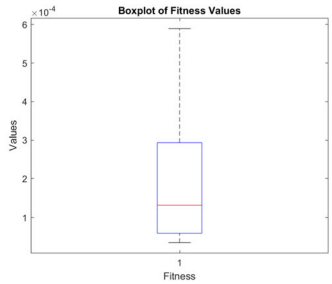

(a) **case 4** : Boxplot of fitness values.

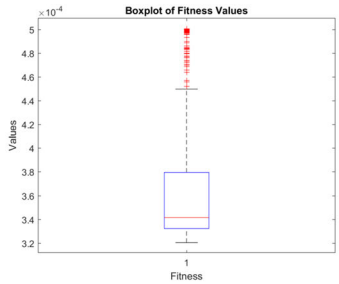

(b) **case 5** : Boxplot of fitness values.

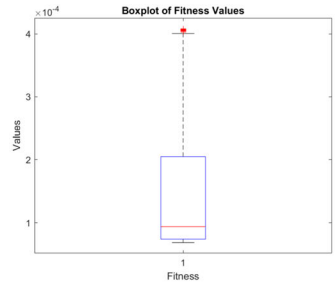

(c) **case 6** : Boxplot of fitness values.

Fig. 21 Boxplots of the fitness values in the cases 1, 2, and 3

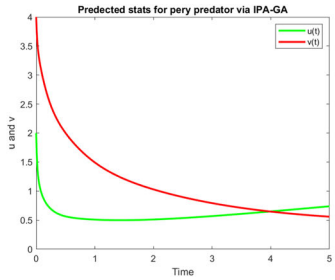

(a) **Case 4** : The behaviour of predator-prey stats via GA-IPA method.

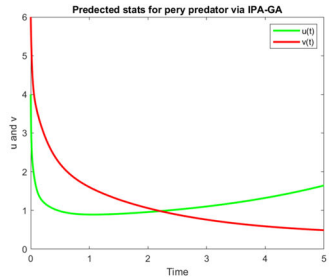

(b) **Case 5** :The behaviour of predator-prey stats via GA-IPA method.

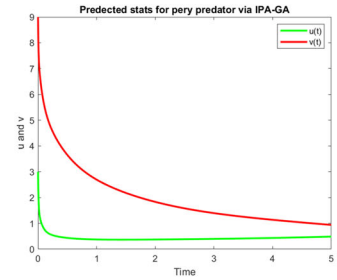

(c) **Case 6** :The behaviour of predator-prey stats via GA-IPA method.

Fig. 22 The behaviour of predator-prey stats via GA-IPA method in each case 4,5 and 6

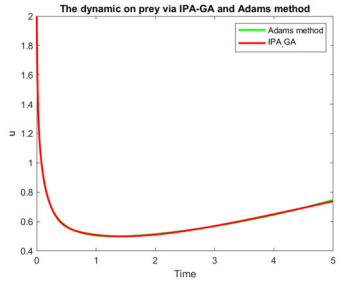

(a) **Case 4** : Comparaison between GA-IPA method and Adams method of the behaviour of prey stats $u(t)$.

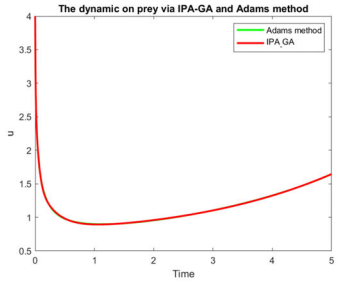

(b) **Case 5** : Comparaison between GA-IPA method and Adams method of the behaviour of prey stats $u(t)$.

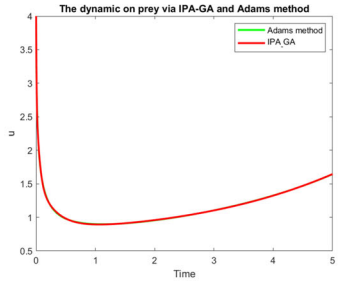

(c) **Case 6** : Comparaison between GA-IPA method and Adams method of the behaviour of prey stats $u(t)$.

Fig. 23 Comparaison between GA-IPA method and Adams method of the behaviour of prey stats $u(t)$. in each case 4,5 and 6

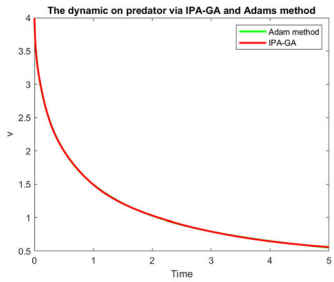

(a) **Case 4** : Comparaison between GA-IPA method and Adams method of the behaviour of predator stats $v(t)$.

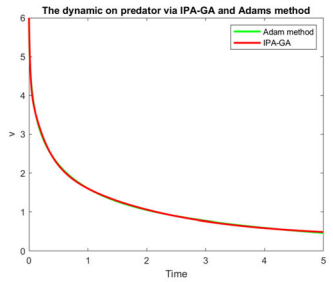

(b) **Case 5** : Comparaison between GA-IPA method and Adams method of the behaviour of predator stat $v(t)$.

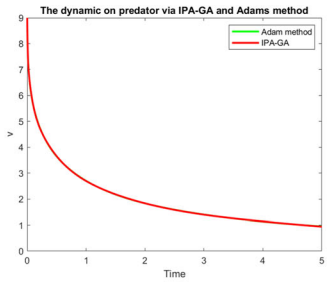

(c) **Case 6** : Comparaison between GA-IPA method and Adams method of the behaviour of predator stats $v(t)$.

Fig. 24 Comparaison between GA-IPA method and Adams method of the behaviour of predator stats $v(t)$. in cases 4, 5, and 6

Fig. 25 The absolute error between the GA-IPA method and the Adams approach for the state $u(t)$

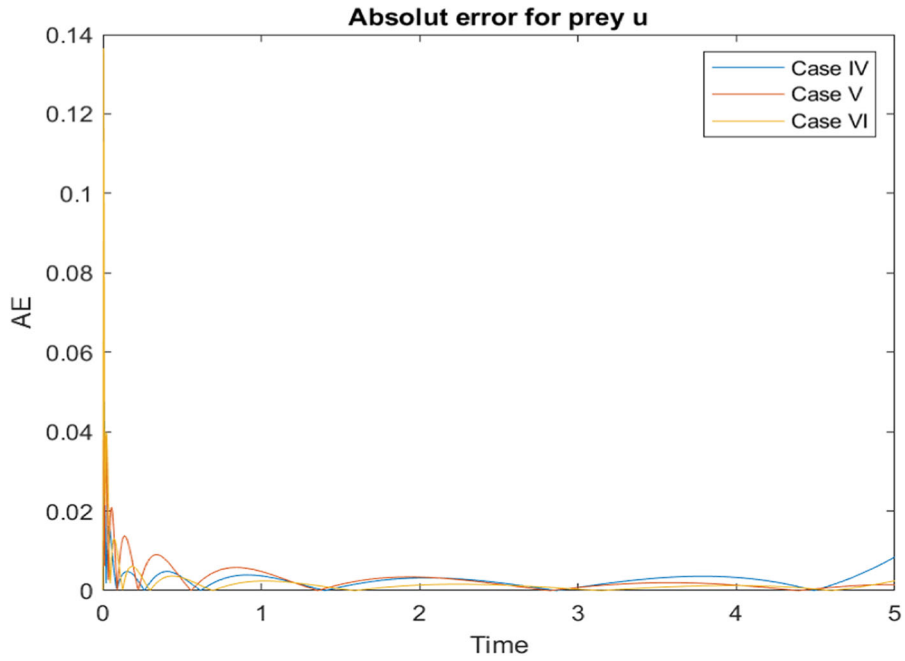

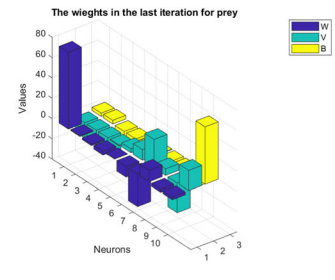

(a) **case 4** : Weights vectors for pery $u(t)$.

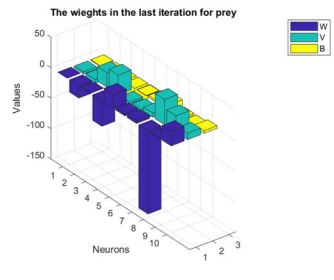

(b) **case 5** : Weights vectors for pery $u(t)$.

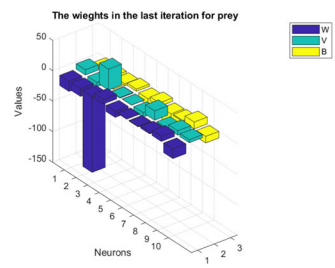

(c) Weights vectors for pery $u(t)$

Fig. 26 The 3D-Histogram shows the values of the weights vectors prey stat in each case 4,5 and 6

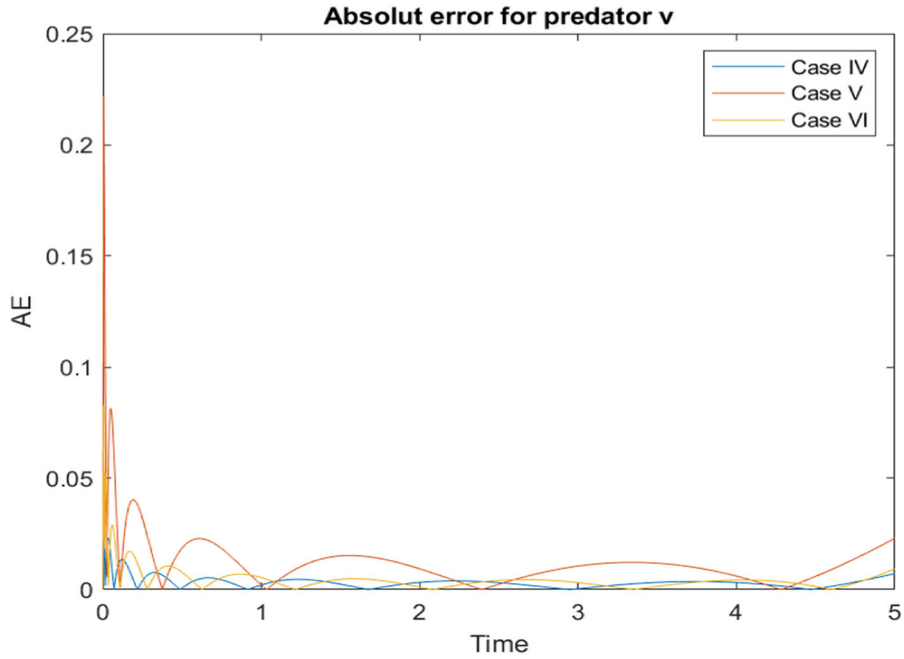

Fig. 27 The absolute error between the GA-IPA method and the Adams approach for the state $v(t)$

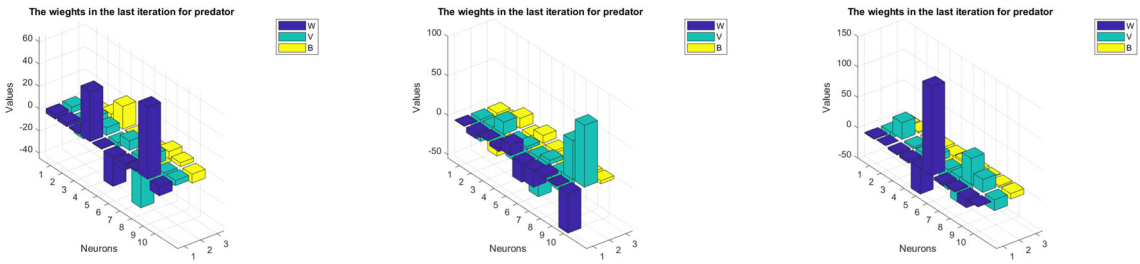

(a) **case 4** : Weights vectors for perdator $v(t)$.

(b) **case 5** : Weights vectors for perdator $v(t)$.

(c) **case 6** : Weights vectors for perdator $v(t)$.

Fig. 28 The 3D-Histogram shows the values of the weights vectors prey stat in each case 4,5 and 6

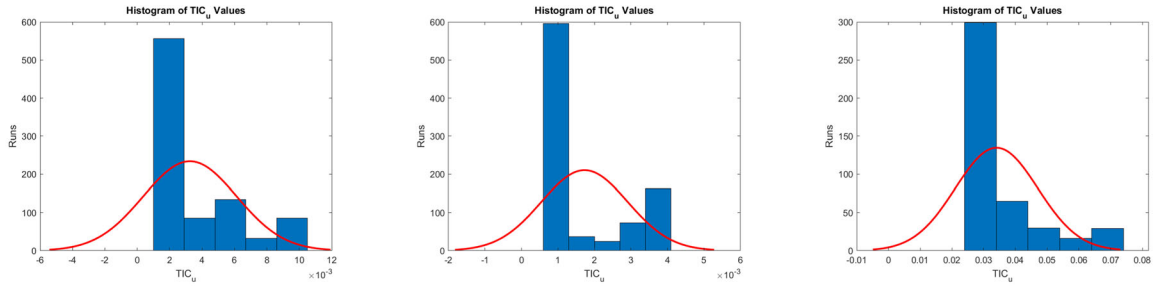

(a) **case 4** : Histogram of TIC values of prey $u(t)$.

(b) **case 5** : Histogram of TIC values of prey $u(t)$.

(c) **case 6** : Histogram of TIC values of prey $u(t)$.

Fig. 29 Histogram of TIC values of prey $u(t)$ in the case 4, 5 and 6

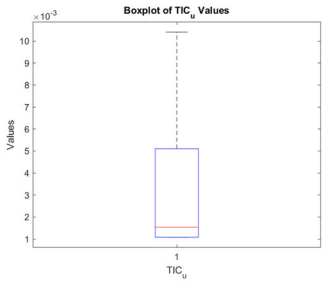

(a) **case 4** : Boxplot of TIC values of prey $u(t)$.

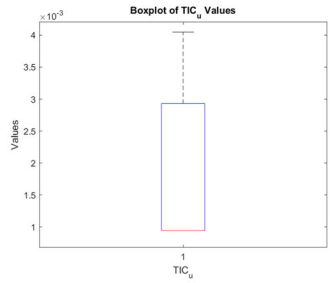

(b) **case 5** : Boxplot of TIC values of prey $u(t)$.

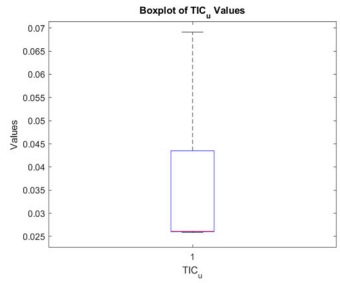

(c) **case 6** : Boxplot of TIC values of prey $u(t)$.

Fig. 30 Boxplot of TIC values of prey $u(t)$ in the case 4,5 and 6

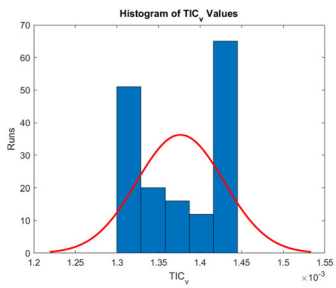

(a) **case 4** : Histogram of TIC values of predator $v(t)$.

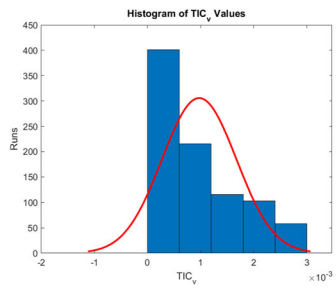

(b) **case 5** : Histogram of TIC values of predator $v(t)$.

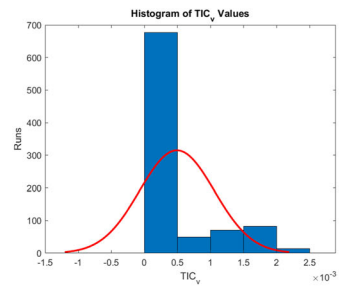

(c) **case 6** : Histogram of TIC values of predator $v(t)$.

Fig. 31 Histogram of TIC values of predator $v(t)$ in the case 4,5 and 6

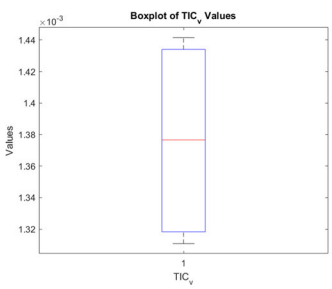

(a) **case 4** : Boxplot of TIC values of predator $v(t)$.

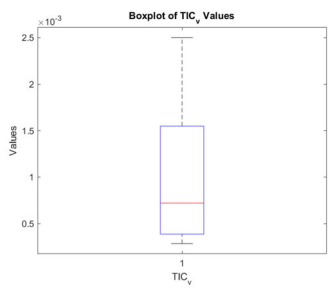

(b) **case 5** : Boxplot of TIC values of predator $v(t)$.

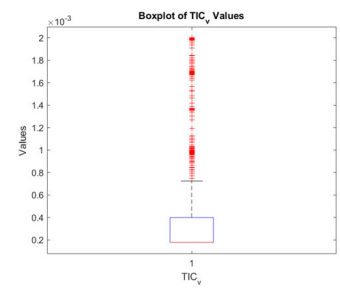

(c) **case 6** : Boxplot of TIC values of predator $v(t)$.

Fig. 32 Boxplot of TIC values of predator $v(t)$ in the case 4,5 and 6 èèèèè

in capturing the system's dynamics with strong agreement between predicted and reference solutions.

In our study we introduce a new artificial neural network (ANN)-based method for solving fractional-order nonlinear predator-prey systems, improving accuracy and efficiency in modeling complex ecological dynamics. The hybrid approach combines ANNs with a Genetic Algorithm-Interior Point Algorithm optimizer for high precision. Results show robustness and reliability, with potential for broader applications in nonlinear biological systems, making this approach a novel development.

4 Conclusion

In this paper, we present a unique neural network-based strategy to solving the nonlinear fractional predator-prey dynamical system (NFPPDS). Our method uses

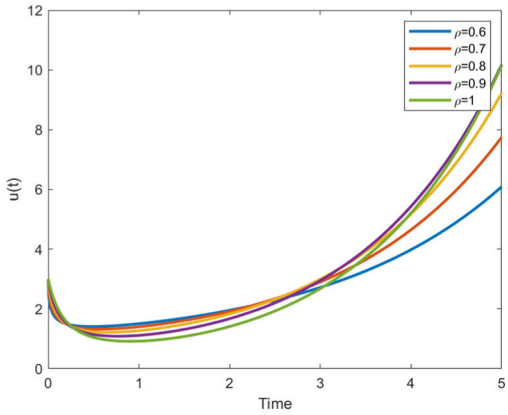

(a) The behaviour of prey using Adams Bash-fourth method.

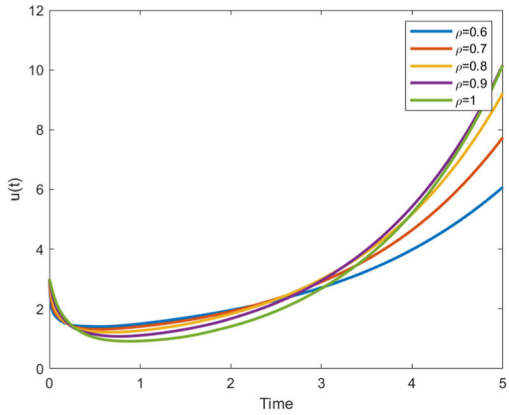

(b) The behaviour of prey using GA-IPA hybrid method.

Fig. 33 The behavior of prey state

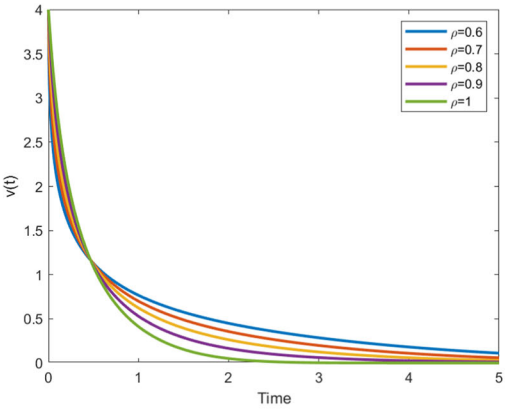

(a) The behaviour of predator using Adams Bash-fourth method.

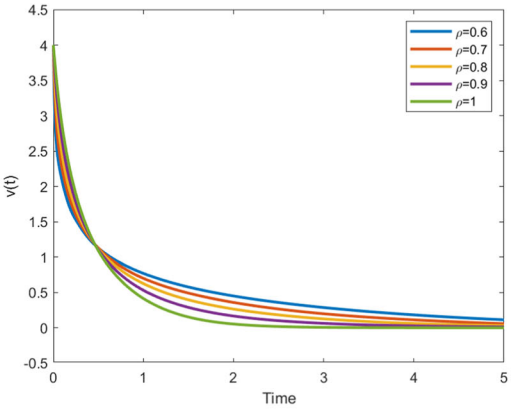

(b) The behaviour of predator using GA-IPA hybrid method.

Fig. 34 The behavior of predator state

a hybrid GA-IPA (Genetic Algorithm-Interior Point Algorithm) optimization framework to generate explicit analytical representations of the projected states. By combining GA's global search capabilities with IPA's local refinement accuracy, our hybrid technique effectively addresses the issues of non-convex optimization in fractional-order systems while maintaining constraint satisfaction and computational economy.

Numerical simulations show that our technique accurately captures complex ecological dynamics, such as memory-dependent interactions and long-term behavioral trends found in fractional predator-prey systems. Validation against the Adams-Bashforth method validates our solutions' robustness, with our strategy achieving higher accuracy and faster convergence in large-scale simulations.

To carefully evaluate our strategy, we carried out a detailed performance analysis utilizing known measures. This includes evaluating numerical accuracy using Mean Square Error (MSE) and Mean Absolute Error (MAE) for all state variables, with a focus on error distribution at important points in population dynamics. Computational efficiency was measured using convergence rates, Processing time, and memory use at various system scales to demonstrate the scalability of our approach.

Comparative investigations with the Adams-Bashforth approach show considerable gains in accu-

racy and stability. The hybrid GA-IPA architecture, when combined with neural networks, achieves a 2% reduction in absolute error (AE) for transient dynamics while improving long-term stability in phase portraiture. Furthermore, our strategy more accurately preserves critical system invariants, resulting in physiologically realistic population thresholds in extended simulations.

The ANN-integrated framework demonstrates remarkable adaptability in handling fractional-order variations. Its unified architecture enables continuous order adaptation within the range $\alpha \in (0, 1)$, allowing efficient generation of solution families across different fractional orders without structural modifications.

Through rigorous metric-based validation and flexible order adaptation, our method establishes itself as a robust tool for fractional ecological modeling. Its advantages are particularly pronounced in studies requiring high-fidelity reproduction of memory-dependent dynamics or investigations of order-dependent system behaviors. Future work may extend this framework to stochastic systems and spatial ecological modeling applications.

Author contributions Nassira Madani: Conducted the research, performed the necessary data collection, and contributed to drafting the manuscript. Zakia Hammouch: Conceptualized the model, supervised the research process, and provided guidance throughout the study. Zakia contributed equally to the development of the research and the manuscript. Necati Ozdemir: Co-supervised the research, offering valuable guidance and insights. Necati contributed equally to the development of the research and the manuscript.

Funding The second author acknowledges the funding provided by Kyung Hee University, Korea.

Data Availability Statement No datasets were generated or analysed during the current study.

Declarations

Competing interests The authors declare no competing interests.

References

1. Abbes, A., Ouannas, A., Shawagfeh, N., Jahanshahi, H.: The fractional-order discrete COVID-19 pandemic model: stability and chaos. Nonlinear Dyn. **111**(1), 965–983 (2023)
2. Alkaabi, H., Alkarbi, N., Almemari, N., Said, S.B., Sabir, Z.: Gudermannian neural network procedure for the nonlinear predator-prey dynamical system. Heliyon. **10**(7), (2024)
3. Baskonus, H.M., Hammouch, Z., Mekkaoui, T., Bulut, H.: Chaos in the fractional order logistic delay system: circuit realization and synchronization. AIP Conf. Proc. **1738**(1), 290005 (2016)
4. Can, E., Sayan, H.H.: Development of fractional sinus pulse width modulation with β gap on three step signal processing. Int. J. Electron. **110**(3), 527–546 (2023)
5. Douven, I., Verbrugge, S.: The adams family. Cognition **117**(3), 302–318 (2010)
6. El Allati, A., Bukbech, S., El Anouz, K., El Allali, Z.: Entanglement versus Bell non-locality via solving the fractional Schrödinger equation using the twisting model. Chaos, Solitons Fractals **179**, 114446 (2024)
7. Yang, Q., Chen, D., Zhao, T., Chen, Y.: Fractional calculus in image processing: a review. Fractional Calculus and Applied Analysis **19**(5), 1222–1249 (2016)
8. Grunwald, A.K.: Uber "begrente" Derivationen und deren Anwedung. Zangew Math und Phys **12**, 441–480 (1867)
9. Hammouch, Z., Jamil, M.O., Unlu, C.: Dynamics investigation and numerical simulation of fractional-order predator-prey model with Holling type II functional response. Discrete and Continuous Dynamical Systems - Series S **18**(5), 1230–1266 (2025)
10. Hamou, A.A., Azroul, E., Hammouch, Z., Lamrani Alaoui, A.: A fractional multi-order model to predict the COVID-19 outbreak in Morocco. Applied Computational Mathematics **20**(1), 177–203 (2020)
11. Jamili, E., Dua, V.: Parameter estimation of partial differential equations using artificial neural network. Comput. Chem. Eng. **147**, 107221 (2021)
12. Junsawang, P., Sabir, Z., Raja, M.A.Z., Salahshour, S., Botmart, T., Weera, W.: Novel computing for the delay differential two-prey and one-predator system. CMC-Comput. Mater. Continua **73**(1), 249–263 (2022)
13. Kumar, S., Chauhan, R.P., Momani, S., Hadid, S.: Numerical investigations on COVID-19 model through singular and non-singular fractional operators. Numerical Methods for Partial Differential Equations **40**(1), e22707 (2024)
14. Liang, Y., Wang, W., Metzler, R., Cherstvy, A.G.: Anomalous diffusion, nonergodicity, non-Gaussianity, and aging of fractional Brownian motion with nonlinear clocks. Phys. Rev. E **108**(3), 034113 (2023)
15. Liu, S., Zhang, Y., Malomed, B.A., Karimi, E.: Experimental realisations of the fractional Schrödinger equation in the temporal domain. Nat. Commun. **14**(1), 222 (2023)
16. Madani, N., Hammouch, Z., Azroul, E.H.: New model of HIV/AIDS dynamics based on Caputo–Fabrizio derivative order: Optimal strategies to control the spread. J. Comput. Sci. 102612, (2025)
17. Mathai, A.M., Saxena, R.K., Haubold, H.J.: The H-function: theory and applications. Springer Science and Business Media (2009)
18. Mehdi, R., Wu, R., Hammouch, Z.: Chaotic bifurcation dynamics in predator–prey interactions with logistic growth and Holling type-II response. Alex. Eng. J. **115**, 119–130 (2025)
19. Mehdi, R., Wu, R., Hammouch, Z.: Chaotic dynamics and control in a discrete predation model with Holling II and prey refuge effects. Chaos: An Interdisciplinary Journal of Nonlinear Science, **35**(6), (2025)
20. Mekkaoui, T., Hammouch, Z.: Approximate analytical solutions to the Bagley-Torvik equation by the fractional itera-

tion method. Annals of the University of Craiova - Mathematics and Computer Science Series **39**(2), 251–256 (2012)
21. Mladenov, V., Mastorakis, N.: Advanced topics on applications of fractional calculus on control problems, system stability and modeling, (2014)
22. Mohammed, M., Alebraheem, J., Tayel, I., Hifzhudin, M.: Dynamics of Competitive Stochastic Predator-Prey Model with Holling Type II under Small Random Immigration. Eur. J. Pure Appl **18**(2), 6097–6097 (2025)
23. Owolabi, K.M., Hammouch, Z.: Mathematical modeling and analysis of two-variable system with noninteger-order derivative. Chaos: An Interdisciplinary Journal of Nonlinear Science, **29**(1), (2019)
24. Rudd, K.: Solving partial differential equations using artificial neural networks (Doctoral dissertation, Duke University) (2013)
25. Ruttanaprommarin, N., Sabir, Z., Said, S.B., Zahoor, M.A., Raja, S.B., Weera, W., Botmart, T.: Supervised neural learning for the predator-prey delay differential system of Holling form-III. AIMS Math **7**(11), 20126–42 (2022)
26. Ruttanaprommarin, N., Sabir, Z., Núñez, R.A.S., Az-Zobi, E., Weera, W., Botmart, T., Zamart, C.: A stochastic framework for solving the predator-prey delay differential model of holling type-III. CMC Comput. Mater. Cont **74**, 5915–5930 (2023)
27. Sabir, Z., Raja, M.A.Z., Khalique, C.M., Unlu, C.: Neuro-evolution computing for nonlinear multi-singular system of third order Emden-Fowler equation. Math. Comput. Simul. **185**, 799–812 (2021)
28. Sabir, Z., Botmart, T., Raja, M.A.Z., Weera, W.: An advanced computing scheme for the numerical investigations of an infection-based fractional-order nonlinear predator-prey system. PLoS ONE **17**(3), e0265064 (2022)
29. Sabir, Z., Botmart, T., Raja, M.A.Z., Sadat, R., Ali, M.R., Alsulami, A.A., Alghamdi, A.: Artificial neural network scheme to solve the nonlinear influenza disease model. Biomed. Signal Process. Control **75**, 103594 (2022)
30. Sabir, Z., Ali, M.R., Sadat, R.: Gudermannian neural networks using the optimization procedures of genetic algorithm and active set approach for the three-species food chain nonlinear model. J. Ambient. Intell. Humaniz. Comput. **14**(7), 8913–8922 (2023)
31. Sabir, Z., Babatin, M.M., Hashem, A.F., Abdelkawy, M.A., Salahshour, S., Umar, M.: Design of stochastic neural networks for the fifth order system of singular engineering model. Eng. Appl. Artif. Intell. **133**, 108141 (2024)
32. Sabir, Z., Rada, T.B., Kassem, Z., Umar, M., Salahshour, S.: A novel radial basis neural network for the Zika virus spreading model. Comput. Biol. Chem. **112**, 108162 (2024)
33. Sabir, Z., Ismail, A., Jaber, A., Khaled, H.E.D., Umar, M., Salahshour, S.: Exploration of deep neural network together with radial basis for the predator-prey nonlinear model. International Journal of Modeling, Simulation, and Scientific Computing (2025)
34. Sabir, Z., Raja, M.A.Z., Umar, M., Salahshour, S., Awan, S.E., Asghar, M.S.: Meta-heuristic tuned with Gudermannian neural network for the singular Neumann, Dirichlet and Neumann-Robin boundary conditions. Multiscale and Multidisciplinary Modeling, Experiments and Design **8**(8), 1–15 (2025
)
35. Sabir, Z., Mehmood, M.A., Umar, M., Salahshour, S., Altun, Y., Arbi, A., Ali, M.R.: A numerical treatment through Bayesian regularization neural network for the chickenpox disease model. Comput. Biol. Med. **187**, 109807 (2025)
36. Sabir, Z., Ismail, T., Sleem, H., Umar, M., Salahshour, S.: A radial basis Bayesian regularization neural network process for the malaria disease model. Knowledge-Based Systems, 113722 (2025)
37. Sabir, Z., Souayeh, B., Umar, M., Salahshour, S., Alfannakh, H., Raju, S.S.K.: A radial basis scale conjugate gradient neural network process for the Zika model with human movement and reservoirs. Chaos, Solitons & Fractals **199**, 116711 (2025)
38. Sabir, Z., Umar, M., Salahshour, S., Saeed, T.: A reliable neural network procedure for the novel sixth-order nonlinear singular pantograph differential model. Mod. Phys. Lett. B **39**(12), 2450473 (2025)
39. Saeed, T., Guirao, J.L., Sabir, Z., Alsulami, H.H., Sánchez, Y.G.: A computational approach to solve the nonlinear biological predator-prey system. Fractals **30**(10), 2240267 (2022)
40. Samko, S.G.: AA Kilbas and 0.1. Marichev. Fractional intearals and derivatives: theory and applications (1993)
41. Sanchez, Y.G., Umar, M., Sabir, Z., Guirao, J.L., Raja, M.A.Z.: Solving a class of biological HIV infection model of latently infected cells using heuristic approach. Discrete and Continuous Dynamical Systems - Series S, **14** (2018)
42. Tarasov, V.E.: Scale-invariant general fractional calculus: Mellin convolution operators. Fractal and Fractional **7**(6), 481 (2023)
43. Umar, M., Sabir, Z., Raja, M.A.Z.: Intelligent computing for numerical treatment of nonlinear predator-prey models. Appl. Soft Comput. **80**, 506–524 (2019)
44. Umar, M., Sabir, Z., Raja, M.A.Z., Amin, F., Saeed, T., Sanchez, Y.G.: Design of intelligent computing solver with Morlet wavelet neural networks for nonlinear predator-prey model. Appl. Soft Comput. **134**, 109975 (2023)
45. Wang, W., Balcerek, M., Burnecki, K., Chechkin, A.V., Janušonis, S., Ślęzak, J., Metzler, R.: Memory-multifractional Brownian motion with continuous correlations. Physical Review Research **5**(3), L032025 (2023)
46. Yaagoub, Z., Danane, J., Hammouch, Z., Allali, K.: Mathematical analysis of a fractional order two strain SEIR epidemic model. Results in Nonlinear Analysis **7**(1), 156–175 (2024)